

1 **Arctic Climate Feedback Response to Local Sea-Ice Concentration and**
2 **Remote Sea Surface Temperature Changes in PAMIP Simulations**

3
4 Matthew T. Jenkins* ¹, Aiguo Dai ¹, Clara Deser ²

5
6 ¹University at Albany, State University of New York, Albany, NY, USA

7 ²National Center for Atmospheric Research, Boulder, CO, USA

8
9 Submitted to: *Climate Dynamics*

10 Date: December 22, 2023

11 1st Revision: May 24, 2024

12
13
14
15
16
17
18
19
20
21
22
23 *Corresponding Author: Matthew T. Jenkins (mtjenkins@albany.edu); ORCID: 0000-0001-5279-1893

24
25
26
27
28
29
30
31
32
33
34
35
36
37
38
39
40
41
42
43
44
45
46
47
48
49
50
51

Abstract

Local and remote processes have been suggested to drive Arctic amplification (AA) – the enhanced warming of the Arctic region relative to other areas under increased greenhouse gases. We use Polar Amplification Model Intercomparison Project (PAMIP) simulations with changes in Arctic sea-ice with fixed global sea surface temperature (SST), or changes in global SST with fixed Arctic sea-ice to untangle the climate response to Arctic sea-ice loss or SST-induced warming, respectively. In response to Arctic sea-ice loss, the surface albedo feedback activates in summer mainly to increase oceanic heat uptake, leading to weak summertime warming. During winter, Arctic sea-ice loss greatly enhances oceanic heat release, which produces Arctic bottom-heavy warming and triggers positive lapse rate and cloud feedbacks, leading to large AA. In contrast, enhanced atmospheric energy convergence into the Arctic becomes the dominant contributor to relatively small AA under global SST-induced warming. Water vapor feedback contributes to Arctic warming but opposes AA due to larger tropical than Arctic moistening under SST-induced warming with fixed Arctic sea-ice. We also find top-heavy to uniform (bottom-heavy) Arctic warming and moistening in the Arctic mid-upper (lower) troposphere in the SST (Arctic sea-ice) perturbation runs, producing a negative-neutral (positive) Arctic lapse rate feedback, respectively. Lastly, we show that the responses to global SST or polar SIC perturbations are linearly separable. Our results suggest that large AA is caused primarily by sea-ice loss and resultant local changes in surface fluxes, while increased poleward energy transport can only produce weak AA under fixed sea ice.

Keywords: Arctic amplification; sea-ice loss; climate feedback; global warming; Arctic warming; ocean heat release; atmospheric energy transport

52 **1. Introduction**

53 The Arctic region warms faster than the rest of the world in response to increased
54 greenhouse gas (GHG) concentrations – a phenomenon known as Arctic amplification (AA)
55 (Serreze and Barry 2011; Walsh 2014; England et al. 2021; Taylor et al. 2022). Many mechanisms
56 have been proposed to explain AA such as surface albedo feedback (Hall 2004; Winton 2006),
57 increased surface downwelling longwave (LW) radiation from enhanced poleward energy
58 transport (Cai 2005; Henry et al. 2021), increased water vapor, or clouds (Ghatak and Miller 2013;
59 Burt et al. 2016; Gong et al. 2017; Monroe et al. 2021), Arctic positive lapse rate feedback (Pithan
60 and Mauritsen 2014; Goosse et al. 2018), and increased upward oceanic energy fluxes due to sea-
61 ice loss (Deser et al. 2010; Kumar et al. 2010; Screen and Simmonds 2010a, b; Boeke and Taylor
62 2018; Dai et al. 2019; Sejas and Taylor 2023). The local and remote mechanisms suggested to
63 contribute to AA are tightly coupled (Feldl et al. 2017b; Henry et al. 2021; Dai and Jenkins 2023),
64 making the exact causes of AA unclear in a fully coupled system. For instance, sea-ice loss largely
65 shapes the spatial patterns of Arctic surface warming and positive lapse rate feedback (Feldl et al.
66 2020; Boeke et al. 2021) by increasing upward surface energy fluxes in autumn and winter that in-
67 turn influences Arctic atmospheric energy convergence and LW cloud feedbacks in non-summer
68 months (Jenkins and Dai 2021). Further, warming in low-mid latitude regions influences Arctic
69 mid-upper tropospheric warming through changes in atmospheric energy convergence into the
70 Arctic, affecting the structure of Arctic warming profiles and lapse rate feedback (Perlwitz et al.
71 2015; Feldl et al. 2020; Hay et al. 2022). Additionally, Liang et al. (2022) showed that AA weakens
72 in the future for greater CO₂ concentrations due to weaker Arctic and global warming differences.
73 Thus, more work is needed to understand how local and remote processes influence Arctic
74 warming and AA.

75 Arctic sea-ice loss plays an essential role in local Arctic warming (Dai et al. 2019; Linke
76 et al. 2023b) and may contribute to warmer winters in northern hemisphere mid-latitude areas (Sun
77 et al. 2016). As sea-ice retreats, increased energy transfer from warm, open water surfaces to the
78 frigid overlying atmosphere during polar night contributes to large AA (Kumar et al. 2010; Deser
79 et al. 2010; Screen and Simmonds 2010a, b; Boeke and Taylor 2018; Taylor et al. 2018; Dai et al.
80 2019; Dai and Jenkins 2023). Exclusion of sea-ice loss effects from models greatly weakens AA.
81 Specifically, Dai et al. (2019) showed that AA weakens in model experiments with 1%/year CO₂

82 increases and fixed SIC for surface flux calculations, and that negligible additional AA will occur
83 after sea-ice completely melts away. Davy and Griewank (2023) confirmed this finding by
84 showing that as the rate of sea-ice loss decreases in the future, concurrent AA weakens. Lastly,
85 previous studies suggest that increased surface heat capacity associated with sea-ice loss affects
86 AA seasonality because more energy input (release) is required to raise (cool) the temperature of
87 open water than sea ice (Dwyer et al. 2012; Hahn et al. 2022; Hu et al. 2022; Sejas et al. 2023).
88 However, the heat capacity of the ocean surface changes little with sea-ice loss as water mass is
89 conserved after ice melts. Thus, the reduced ice-insulation effect associated with sea-ice loss is the
90 main driver of large cold season AA (Dai and Jenkins 2023).

91 Another process underlying AA is the lapse rate feedback that depends on local vertical
92 warming structures (Pithan and Mauritsen 2014; Linke et al. 2023a; Zhou et al. 2023). Under a
93 bottom-heavy warming profile, outgoing LW radiation at the top of the atmosphere (TOA) is
94 reduced relative to vertically uniform warming, thereby enhancing surface warming (Boeke et al.
95 2021; Dai and Jenkins 2023). In contrast, a top-heavy warming profile, as seen in the tropics,
96 suppresses surface warming by increasing outgoing LW radiation (Colman and Soden 2021). The
97 lapse rate feedback has been considered as a major contributor to AA due to its large Arctic versus
98 tropical warming effect (Pithan and Mauritsen 2014; Goosse et al. 2018; Hahn et al. 2021).
99 Previous studies have attributed Arctic bottom-heavy warming and the resultant positive lapse rate
100 feedback to high lower-tropospheric stability, which effectively traps warming at the surface
101 (Bintanja et al. 2011; Pithan and Mauritsen 2014). However, recent studies suggest that Arctic
102 lapse rate feedback is strongly correlated with surface warming patterns and sea-ice loss (Feldl et
103 al. 2020; Boeke et al. 2021; Jenkins and Dai 2021) rather than stability strength (Jenkins and Dai
104 2022; Dai and Jenkins 2023). Remote processes, such as enhanced moist static energy convergence
105 into the Arctic, may also influence Arctic lapse rate feedback by favoring warming in the mid-
106 upper troposphere (Feldl et al. 2020), leading to negative lapse rate feedback.

107 During summer, surface albedo and water vapor feedbacks activate in the Arctic in
108 response to greenhouse gas (GHG) forcing. The surface albedo feedback makes a large positive
109 contribution to Arctic energy imbalance in summer (Hall 2004; Winton 2006; Pithan and
110 Mauritsen 2014; Goosse et al. 2018; Hahn et al. 2021); however, most of the enhanced shortwave
111 (SW) absorption preferably warms the ocean mixed layer rather than near-surface air (Dai 2021;

112 Dai and Jenkins 2023). Additionally, water vapor feedback has been suggested to contribute to
113 Arctic *warming* (Ghatak and Miller 2013; Gong et al. 2017) but oppose Arctic *amplification* due
114 to larger moistening in tropical regions than polar areas under increased GHGs (Pithan and
115 Mauritsen 2014; Hahn et al. 2021). Jenkins and Dai (2022) showed that water vapor feedback and
116 sea-ice loss spatial patterns are weakly correlated in ERA5 reanalysis data, but they did not
117 quantify the underlying local and remote drivers of Arctic water vapor feedback. An improved
118 understanding of Arctic water vapor feedback is needed as it enhances Arctic surface warming and
119 melts sea ice, indirectly contributing to AA through the sea-ice feedback (Dai et al. 2019; Dai and
120 Jenkins 2023). Moreover, water vapor feedback may interact with other processes by changing
121 patterns of atmospheric latent energy transport (Chung and Feldl 2023) or amplifying other climate
122 feedbacks (Beer and Eisenman 2022).

123 Cloud feedback impacts TOA and surface energy fluxes (Wetherald and Manabe 1988),
124 but their response to local and remote processes is not fully understood. Previous studies have
125 found an increase in local Arctic low cloud amounts and cloud water content in response to local
126 sea-ice loss due to strong cold season ocean-atmosphere coupling (Schweiger et al. 2008; Kay and
127 Gettelman 2009; Eastman and Warren 2010; Liu et al. 2012; Taylor et al. 2015; Kay et al. 2016;
128 Morrison et al. 2018, 2019; Jenkins and Dai 2022; Jenkins et al. 2023; Taylor and Monroe 2023).
129 Increased surface downwelling LW radiation from local Arctic cloud increases slows sea ice
130 growth during Arctic autumn and winter, lengthening exposure of open water surfaces to heat the
131 overlying air during the cold season (Monroe et al. 2021). Nonlocal cloud feedbacks may also
132 contribute to Arctic warming and AA by affecting remote surface warming patterns and thus
133 atmospheric energy transport into the Arctic (Vavrus et al. 2004; Middlemas et al. 2020).

134 Increased energy transport from midlatitudes into the Arctic has been suggested to
135 influence AA (Cai 2005; Roe et al. 2015; Feldl et al. 2017b; Soldatenko 2021). Without sea-ice
136 loss and associated surface heating, enhanced poleward atmospheric energy transport produces
137 only weak AA in model simulations (Alexeev et al. 2005; Merlis and Henry 2018; Henry et al.
138 2021). On the other hand, inclusion of sea-ice loss effects in model simulations reduces
139 atmospheric energy transport into the Arctic due to decreased temperature gradients between
140 middle and high latitudes (Hwang et al. 2011; Jenkins and Dai 2021; Audette et al. 2021; Hahn et
141 al. 2023). However, Cardinale and Rose (2023) showed that an increase in the fraction of the Arctic

142 energy convergence used to heat the surface may overcome the total decrease in Arctic energy
143 convergence, contributing to winter Arctic warming. Inhomogeneous spatial patterns of radiative
144 forcing also influence atmospheric poleward energy transport (Stuecker et al. 2018; Virgin and
145 Smith 2019). When radiative forcing is negative in the Arctic, atmospheric poleward energy
146 transport increases to offset the energy imbalance, inducing small AA (Virgin and Smith 2019).
147 Additionally, Stuecker et al. (2018) found that atmospheric energy transport became an important
148 contributor to AA in response to radiative forcing applied only in midlatitudes in fully coupled
149 simulations, but they did not examine the effects of sea-ice loss in shaping the Arctic warming in
150 response to such forcing.

151 The relative importance of sea-ice loss, positive climate feedbacks, and atmospheric energy
152 transport in shaping AA is still debated and merits further investigation. Arctic climate feedbacks
153 have been estimated in coupled model simulations (Pithan and Mauritsen 2014; Sejas et al. 2014;
154 Goosse et al. 2018; Stuecker et al. 2018; Previdi et al. 2020; Hahn et al. 2021); however, the
155 influence of local sea-ice loss or remote SST warming on climate feedbacks cannot be explicitly
156 quantified in a fully coupled system. To address these points, we use atmosphere-only simulations
157 from the Polar Amplification Model Intercomparison Project (PAMIP; Smith et al. 2019) to
158 answer the following questions:

- 159 1. What are the impacts of local Arctic SIC changes through enhanced oceanic heating of the
160 atmosphere or global SST changes and background warming in atmosphere-only model
161 simulations on Arctic surface warming, AA, radiative climate feedbacks, and atmospheric
162 energy transport?
- 163 2. Do the individual responses to SST warming or Arctic SIC loss sum to the total response
164 to the combined influences of SST warming and Arctic SIC loss occurring simultaneously?

165 The PAMIP experiments allow us to separate the climate response to perturbations in local sea ice
166 or remote SST changes in model simulations under fixed GHG concentrations. The SST
167 perturbation runs represent the climatic effects of background global warming without large AA,
168 while the Arctic SIC change simulations show the impact from Arctic sea-ice loss without
169 background global warming.

170 **2. Methods**

171 *2.1 PAMIP experiments*

172 We investigate how changes in global SST and/or local SIC impact Arctic surface
173 warming, AA, climate feedbacks, and atmospheric energy transport using PAMIP atmosphere-
174 only time slice experiments (Table 1; Smith et al. 2019). PAMIP experiment 1.1 (pdSST-pdSIC)
175 serves as the control run where global SST and polar (i.e., Arctic and Antarctic) SIC fields are
176 fixed at their present-day (pd) (i.e., year 2000) values. To isolate the response to global SST
177 changes, we compare the pdSST-pdSIC run to PAMIP experiments 1.3 (piSST-pdSIC) and 1.4
178 (futSST-pdSIC) where polar (i.e., Arctic and Antarctic) SIC remains fixed at present-day
179 conditions and SSTs over open water surfaces are set to preindustrial (pi) and future (fut) states
180 (defined below), respectively. Likewise, we difference the pdSST-pdSIC run with PAMIP
181 experiments 1.5 (pdSST-piArcSIC) and 1.6 (pdSST-futArcSIC) where SSTs outside the Arctic
182 region are fixed at their present-day values and Arctic SIC is changed to preindustrial and future
183 states to separate the impacts of sea-ice loss from other forcings. For the pdSST-piArcSIC and
184 pdSST-futArcSIC simulations, SSTs are specified at their preindustrial or future values in regions
185 where preindustrial or future SIC deviates by more than 10% of the present-day state, respectively
186 (Smith et al. 2019).

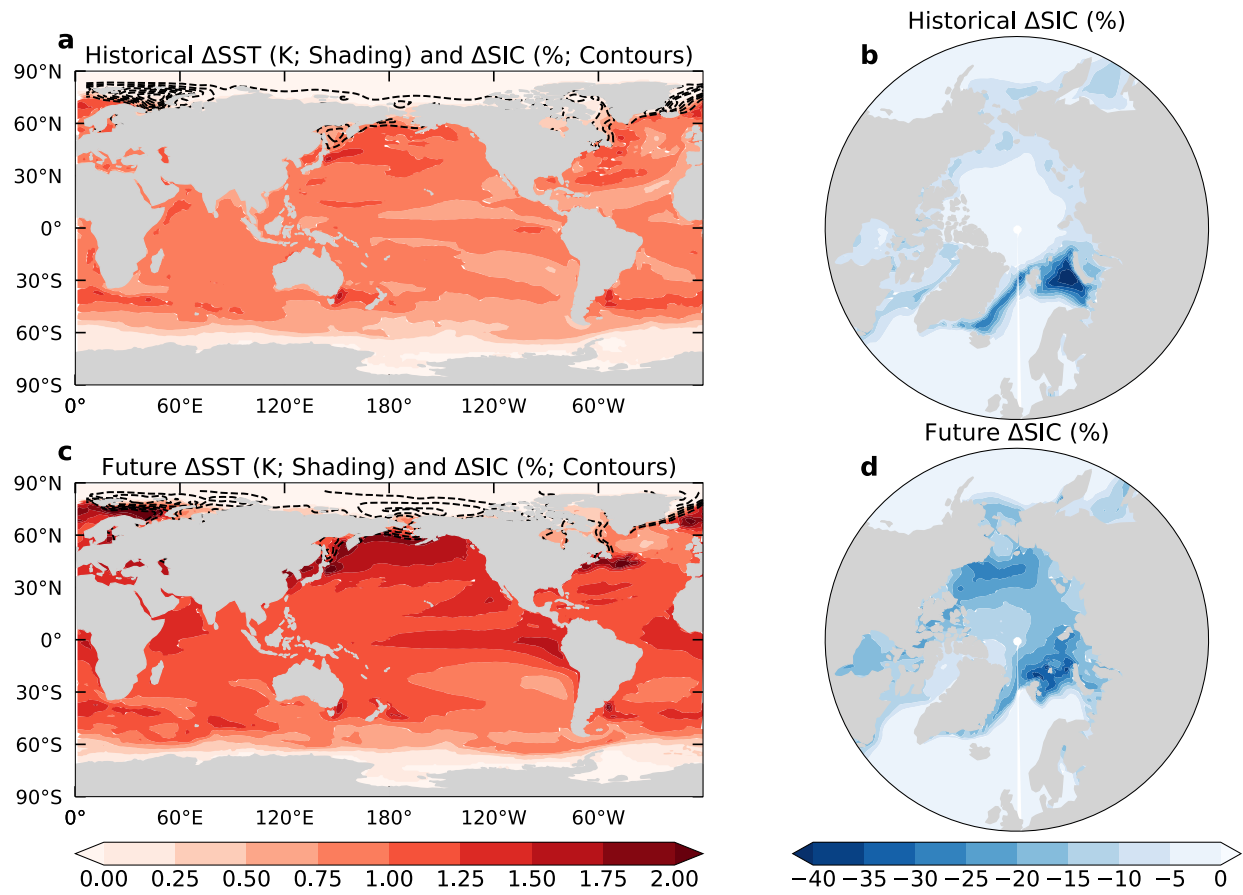
187 Figure 1 shows the maps of prescribed SST and SIC changes for the preindustrial (Fig. 1a,
188 b) or future (Fig. 1c, d) cases. To facilitate comparison with the future changes, which are relative
189 to present-day, the historical changes are computed as present-day minus preindustrial in Fig. 1
190 and all other figures. We also compute the difference between pdSST-pdSIC and experiment 1.2
191 (piSST-piSIC; referred to as TOTAL) where global SSTs and polar SIC are changed
192 simultaneously to their preindustrial states. We compare the results from TOTAL to the difference
193 between pdSST-pdSIC and the sum of piSST-pdSIC, pdSST-piArcSIC and pdSST-piAntSIC
194 (referred to as SUM) to assess the linearity of the total climate response to both polar SIC and
195 global SST changes. The preindustrial, present-day, and future time periods correspond to
196 estimated Arctic SIC and/or global SST conditions under global-mean surface temperatures of
197 13.67°C, 14.24°C, and 15.67°C, respectively (Smith et al. 2019), which correspond to a historical
198 warming of 0.57°C and a future warming of 1.43°C relative to present-day. Their corresponding
199 SIC changes are also much larger for the future case than the historical case (Fig. 1). Present-day
200 SST and SIC fields are based on the 1979-2008 climatology from the Hadley Center Sea Ice and

201 Sea Surface Temperature dataset (HadISST; Rayner et al. 2003). Preindustrial and future SST and
 202 SIC fields are derived from the CMIP5 historical and RCP8.5 experiments for 31 models,
 203 respectively (Smith et al. 2019). See Appendix A of Smith et al. (2019) for more details.

204 **Table 1.** Summary of PAMIP experiments used in the analysis (from Smith et al. 2019).

| Model Simulation | Full Name | Description |
|-------------------------|--|--|
| 1.1 pdSST-pdSIC | Present day sea surface temperature Present-day sea-ice concentration | Year 2000 global SST and polar SIC; control run. |
| 1.2 piSST-piSIC | Preindustrial sea surface temperature Preindustrial sea-ice concentration | Historical global SST and polar SIC; assesses total climate response to SST and SIC changes. |
| 1.3 piSST-pdSIC | Preindustrial sea surface temperature Present-day sea-ice concentration | Historical (1.3) and future (1.4) global SST with polar SIC fixed at year 2000 conditions; assesses role of background warming without sea-ice feedback. |
| 1.4 futSST-pdSIC | Future sea surface temperature Present-day sea-ice concentration | |
| 1.5 pdSST-piArcSIC | Present-day sea surface temperature Preindustrial sea-ice concentration | Historical (1.5) and future (1.6) Arctic SIC with global SST fixed at year 2000 conditions; assesses role of Arctic sea-ice feedback without background warming. |
| 1.6 pdSST-futArcSIC | Present-day sea surface temperature Future sea ice concentration | |
| 1.7 pdSST-piAntSIC | Present-day SST Preindustrial Antarctic SIC | Historical Antarctic SIC with global SST fixed at year 2000 conditions; assesses role of Antarctic sea-ice feedback without background warming. |

205



206

207 **Fig. 1.** (a, c) Annual mean changes in SST (K; shading) and Arctic SIC (%) (contours; interval 5%)
 208 for the (a) historical (present-day minus preindustrial) and (c) future warming (future minus
 209 present-day) cases. Changes in SIC for the (b) historical and (d) future cases are shown as shading
 210 in (b) and (d) for clarity.

211 We use monthly-mean output from five models (i.e., AWI-CM1-1-MR, CESM2, CNRM-
 212 CM6-1, CanESM5, IPSL-CM6A-LR) that provided the necessary fields for our analysis. AWI-
 213 CM1-1-MR and CNRM-CM6-1 did not output the necessary variables for some calculations in
 214 piSST-piSIC (i.e., TOTAL) and is excluded in our comparison of piSST-piSIC to the sum of
 215 piSST-pdSIC, pdSST-piArcSIC, and pdSST-piAntSIC (i.e., SUM). Each model and experiment
 216 are initialized on 1 April 2000 and are run for 14-months, discarding the first two months as spin-
 217 up (Smith et al. 2019). To improve robustness of the results, we analyze the ensemble mean of the
 218 100 ensemble runs with varied initial conditions for each model and experiment as atmospheric
 219 internal variability can mask the climatic response to SIC or SST changes (Screen et al. 2014). We
 220 define the Arctic region as the area poleward of 67°N following previous work (e.g., Dai et al.
 221 2019; Jenkins and Dai 2022) because most Arctic sea-ice exists poleward of this latitude and the

222 Arctic is mostly ocean surface in this region. We exclude land surfaces in our Arctic regional
 223 averages because surface warming is strongest over oceanic areas (Boeke and Taylor 2018; Dai et
 224 al. 2019) but inclusion of land areas does not qualitatively affect our results. Globally averaged
 225 fields include both land and ocean surfaces. For this study, we calculate AA as the difference
 226 between Arctic (excluding land) and global surface air temperature (ΔT_{as}) changes ($AA =$
 227 $\Delta T_{as,ARCTIC} - \Delta T_{as,GLOBAL}$) rather than as the ratio of Arctic to global warming to avoid dividing by
 228 near-zero values for global-mean surface air temperature changes.

229 2.2 Energy budgets

230 The vertically integrated energy budget equation (Eq. 1) for an atmospheric column
 231 accounts for the net TOA radiative flux (R_{TOA}^\downarrow ; positive downward), net surface energy flux (R_{SFC}^\downarrow ;
 232 positive downward), change in local energy storage in the atmospheric column ($\frac{\partial E}{\partial t}$), and horizontal
 233 convergence of energy ($-\nabla \cdot \mathbf{F}_A$) (Trenberth 1997; Fasullo and Trenberth 2008):

$$234 \quad \frac{\partial E}{\partial t} = R_{TOA}^\downarrow - R_{SFC}^\downarrow - \nabla \cdot \mathbf{F}_A \quad , \quad (1)$$

235 where

$$236 \quad E = \frac{1}{g} \int_{p_{TOA}}^{p_s} (c_p T + Lq + gz) dp. \quad (2)$$

237 In Eq. (2), E is the vertically integrated moist static energy, where $c_p T$, Lq , and gz denote
 238 atmospheric internal energy, latent energy, and potential energy, respectively. Atmospheric kinetic
 239 energy storage is small and is not included in Eq. (2), following previous studies (Oort and Vonder
 240 Haar 1976; Trenberth and Solomon 1994). For the flux terms, we calculate R_{TOA}^\downarrow and R_{SFC}^\downarrow as:

$$241 \quad R_{TOA}^\downarrow = ASR^\downarrow - OLR^\uparrow \quad (3)$$

$$242 \quad R_{SFC}^\downarrow = SW_{NET,SFC}^\downarrow - LW_{NET,SFC}^\uparrow - SH^\uparrow - LH^\uparrow \quad (4)$$

243 where ASR^\downarrow , OLR^\uparrow , $SW_{NET,SFC}^\downarrow$, $LW_{NET,SFC}^\uparrow$, SH^\uparrow , and LH^\uparrow are the TOA absorbed SW radiation
 244 (positive downward), TOA outgoing LW radiation (positive upward), net surface SW radiation
 245 (positive downward), net surface LW radiation (positive upward), surface sensible and latent heat
 246 flux (positive upward), respectively. Note that the latent heat term does not account for the latent
 247 heat consumed in snow melt in Eq. (4). To estimate oceanic heat uptake (OHU), we calculate the

248 net surface energy flux (Eq. 4) over ocean surfaces only. For the simulations with perturbed global
 249 SST and fixed Arctic SIC, changes in OHU implicitly include changes in oceanic energy
 250 convergence in addition to oceanic heat storage changes as historical and future SST values are
 251 obtained using a coupled atmosphere-ocean. In contrast, the OHU term in the simulations with
 252 perturbed Arctic SIC and fixed global SST is dominated by seasonal oceanic heat storage changes
 253 (Dai 2021; Hu et al. 2022) as oceanic heat transport changes little with fixed SST values.

254 We compute the horizontal atmospheric energy convergence ($-\nabla \cdot \mathbf{F}_A$) by rearranging the
 255 terms in Eq. (1) to obtain:

$$256 \quad -\nabla \cdot \mathbf{F}_A = R_{SFC}^\downarrow - R_{TOA}^\downarrow + \frac{\partial E}{\partial t}. \quad (5)$$

257 Eq. (5) shows that the net convergence of the horizontal energy flux (in $W\ m^{-2}$) into a column is
 258 linked to the difference between the energy absorbed at the surface and net TOA radiation, and
 259 changes in local energy storage. Note that the local energy storage term is calculated using a
 260 month-to-month time derivative of Eq. (2) and is necessary for calculating monthly energy
 261 convergence but sums to zero in the annual mean. We also calculate the atmospheric energy
 262 transport (AET; in PW) into the region north of a given latitude (ϕ) by taking the area integral of
 263 the net energy convergence over the region following previous studies (Hwang and Frierson 2010;
 264 Feldl et al. 2017a):

$$265 \quad AET(\phi) = \int_{\phi}^{\pi/2} \int_0^{2\pi} \left(R_{SFC}^\downarrow - R_{TOA}^\downarrow + \frac{\partial E}{\partial t} \right) a^2 \cos \phi \, d\gamma d\phi. \quad (6)$$

266 In Eq. (6), a is the radius of Earth ($\sim 6.371 \times 10^6$ m), γ is the longitude, and ϕ is the latitude.
 267 $AET(\phi)$ represents the total energy crosses the latitude circle at ϕ (positive northward). For our
 268 Arctic region, $\phi=67^\circ N$.

269 2.3 Climate feedback calculations

270 The response of the atmospheric energy budget to a climate perturbation, assuming
 271 negligible changes in atmospheric energy storage, is:

$$272 \quad \Delta R_{TOA}^\downarrow - \Delta R_{SFC}^\downarrow - \Delta(\nabla \cdot \mathbf{F}_A) = 0 \quad (7)$$

273 where $\Delta R_{TOA}^\downarrow$, $\Delta R_{SFC}^\downarrow$, and $\Delta(\nabla \cdot \mathbf{F}_A)$ are changes in the net TOA radiative flux, net surface energy
 274 flux, and atmospheric horizontal energy convergence at each grid point, respectively (Stuecker et

275 al. 2018; Hahn et al. 2021; Zhou et al. 2023). We use the Pendergrass et al. (2018) CESM1-CAM5
 276 radiative kernels to decompose changes in the TOA net radiative flux into individual contributions
 277 from changes in surface albedo (ΔR_α), water vapor (ΔR_q), air temperature (ΔR_T), and clouds (ΔR_C):

$$278 \quad \Delta R_{TOA}^\downarrow = \Delta R_\alpha^\downarrow + \Delta R_q^\downarrow + \Delta R_T^\downarrow + \Delta R_C^\downarrow. \quad (8)$$

279 GHG concentrations remain fixed at year 2000 levels in the PAMIP simulations, so we exclude an
 280 effective radiative forcing term from our TOA flux change decomposition. The annual-mean
 281 residual TOA radiative flux changes (i.e., the difference between the actual TOA radiation change
 282 and sum of radiative feedback contributions in Eq. (8)) are 0.29 W m^{-2} and 0.27 W m^{-2} for historical
 283 and future global SST changes with fixed SIC, and 1.15 W m^{-2} and 1.79 W m^{-2} for historical and
 284 future Arctic SIC with fixed global SST. These residual TOA fluxes account for errors related to
 285 the radiative kernels and physical processes not included in our feedback decomposition. We also
 286 normalize the TOA flux changes in Eq. (8) by the annual-mean local surface air temperature
 287 change (ΔT_{as}) to calculate the climate feedback parameter (λ_i) for each variable using:

$$288 \quad \sum_i \lambda_i = \lambda_\alpha + \lambda_q + \lambda_T + \lambda_C = \frac{\Delta R_\alpha^\downarrow + \Delta R_q^\downarrow + \Delta R_T^\downarrow + \Delta R_C^\downarrow}{\Delta T_{as}} \quad (9)$$

289 For clarity, we use the term *feedback* to refer to the unnormalized TOA radiative flux changes
 290 (units: W m^{-2}) in Eq. (8) and *feedback parameter* to refer to the normalized TOA radiative fluxes
 291 (units: $\text{W m}^{-2} \text{K}^{-1}$) in Eq. (9).

292 Radiative kernels are computed by perturbing one climate variable in a radiative transfer
 293 model and keeping all other variables fixed to produce a TOA radiative flux response, which is
 294 divided by the amount of the perturbed variable change to derive the TOA flux change per unit
 295 variable change (Soden et al. 2008). To calculate the surface albedo feedback, we compute the
 296 product of the surface albedo kernel (K_α) and changes in surface albedo ($\Delta\alpha$): $\Delta R_\alpha = K_\alpha * \Delta\alpha$. For
 297 water vapor (Eq. 10) and temperature (Eq. 11) feedbacks, we vertically integrate the product of
 298 the kernel and change in each respective variable from the surface (p_s) to the tropopause (p_{TOA}):

$$299 \quad \Delta R_q = \int_{p_{TOA}}^{p_s} K_q * \Delta \ln(q) dp \quad (10)$$

$$300 \quad \Delta R_T = K_{Ts} * \Delta T_{as} + \int_{p_{TOA}}^{p_s} K_{Ta} * \Delta T_a dp \quad (11)$$

301 where q and T_a represent specific humidity and air temperature, respectively. Radiative emissions
 302 from water vapor scale with the natural logarithm of specific humidity, so we use $\Delta \ln(q)$ in Eq.
 303 (10) as done previously (Shell et al. 2008). Also, note that the temperature feedback accounts for
 304 changes in surface temperature, which is computed by taking the product of the surface
 305 temperature kernel (K_{Ts}) and change in surface air temperature (ΔT_{as}) (Block and Mauritsen 2013;
 306 Jenkins and Dai 2021). Further, we assume that the tropopause pressure increases with latitude
 307 from 100 hPa at the equator to 300 hPa at the poles following Pithan and Mauritsen (2014) to mask
 308 out the stratosphere. To calculate Planck and lapse rate feedbacks, we separate the temperature
 309 feedback (ΔR_T) into a component associated with vertically uniform warming equal to that of the
 310 surface (Planck feedback; ΔR_{PL}) and deviations from the vertically uniform warming profile (lapse
 311 rate feedback; ΔR_{LR}):

$$\begin{aligned}
 312 \quad \Delta R_T &= \Delta R_{PL} + \Delta R_{LR} \\
 313 \quad &= K_{Ts} * \Delta T_{as} + \int_{p_{TOA}}^{p_s} K_{Ta} * \Delta T_{as} dp + \int_{p_{TOA}}^{p_s} K_{Ta} * (\Delta T_a - \Delta T_{as}) dp \quad (12)
 \end{aligned}$$

314 More details on Planck and lapse rate feedback calculations are provided in Jenkins and Dai (2021)
 315 and Dai and Jenkins (2023).

316 The change in cloud radiative forcing (ΔCRF) – the difference between all-sky and clear-
 317 sky radiative fluxes – provides a simple estimate of the energetic effects of clouds but does not
 318 represent cloud feedback as other processes also affect this difference (Soden et al. 2008; Block
 319 and Mauritsen 2013). To compute cloud feedback (ΔR_C), we subtract a cloud masking (CM) term
 320 from the ΔCRF to account for the effects of changes in surface albedo, temperature, and water
 321 vapor on ΔCRF (Soden et al. 2008):

$$322 \quad \Delta R_C = \Delta CRF - CM \quad (13)$$

323 where

$$324 \quad CM = (K_\alpha - K_\alpha^C) * \Delta \alpha + \int_{p_{TOA}}^{p_s} (K_{Ta} - K_{Ta}^C) * \Delta T_a dp + \int_{p_{TOA}}^{p_s} (K_q - K_q^C) * \Delta \ln(q) dp. \quad (14)$$

325 In Eq. (14) K_i and K_i^C are the all-sky and clear-sky kernels for surface albedo (α), air temperature
 326 (T_a), and water vapor (q). GHG concentrations are fixed in the PAMIP runs so we exclude a GHG
 327 masking term in Eq. (14).

328 2.4 Potential warming contribution estimates

329 To facilitate comparison, we quantify climate feedbacks, oceanic heat uptake, and
330 horizontal atmospheric energy convergence in terms of their *potential* warming contributions
331 following previous studies (e.g., Pithan and Mauritsen 2014; Goosse et al. 2021; Stuecker et al.
332 2018; Hahn et al. 2021). The potential warming contribution from the i th climate feedback ($\Delta T_i = \Delta R_i$
333 $/\bar{\lambda}_{PL}$, in K) represents a hypothetical warming amount needed to rebalance the TOA energy flux
334 change ($\Delta R_i = \lambda_i \Delta T_{as}$) through the negative Planck feedback at a new *equilibrium* state. Similarly,
335 we can scale the other flux changes to estimate their potential warming contributions, and the total
336 potential warming amount (ΔT) is estimated as (Goosse et al. 2018; Hahn et al. 2021):

$$337 \quad \Delta T = -\frac{\sum_i \lambda_i \Delta T_{as}}{\bar{\lambda}_{PL}} - \frac{\lambda'_{PL} \Delta T_{as}}{\bar{\lambda}_{PL}} - \frac{\Delta(-\nabla \cdot F_A)}{\bar{\lambda}_{PL}} - \frac{\Delta OHU}{\bar{\lambda}_{PL}} \quad (15)$$

338 where $\bar{\lambda}_{PL}$ (in $\text{W m}^{-2} \text{K}^{-1}$) is the global-mean Planck feedback parameter and λ'_{PL} is the deviation of
339 the local (λ_{PL}) Planck feedback parameter from its global mean: $\lambda'_{PL} = \lambda_{PL} - \bar{\lambda}_{PL}$. As noted by
340 Dai and Jenkins (2023), this estimated warming amount often does not represent a real warming
341 contribution as the TOA flux change (ΔR_i) may not be used to directly raise surface air temperature
342 or the temperature response may be delayed. We average the terms in Eq. (15) over the Arctic
343 (67° - 90°N) and the tropics (23.5°S - 23.5°N) to estimate the potential warming contribution of each
344 process to surface warming and AA as done previously (Pithan and Mauritsen 2014; Goosse et al.
345 2018; Stuecker et al. 2018; Hahn et al. 2021). We define the tropical region as 23.5°S - 23.5°N as
346 these are the latitude bands between the Tropic of Capricorn and Tropic of Cancer; however,
347 averaging over other latitude ranges for the tropics (e.g., 30°S - 30°N) does not impact the results.

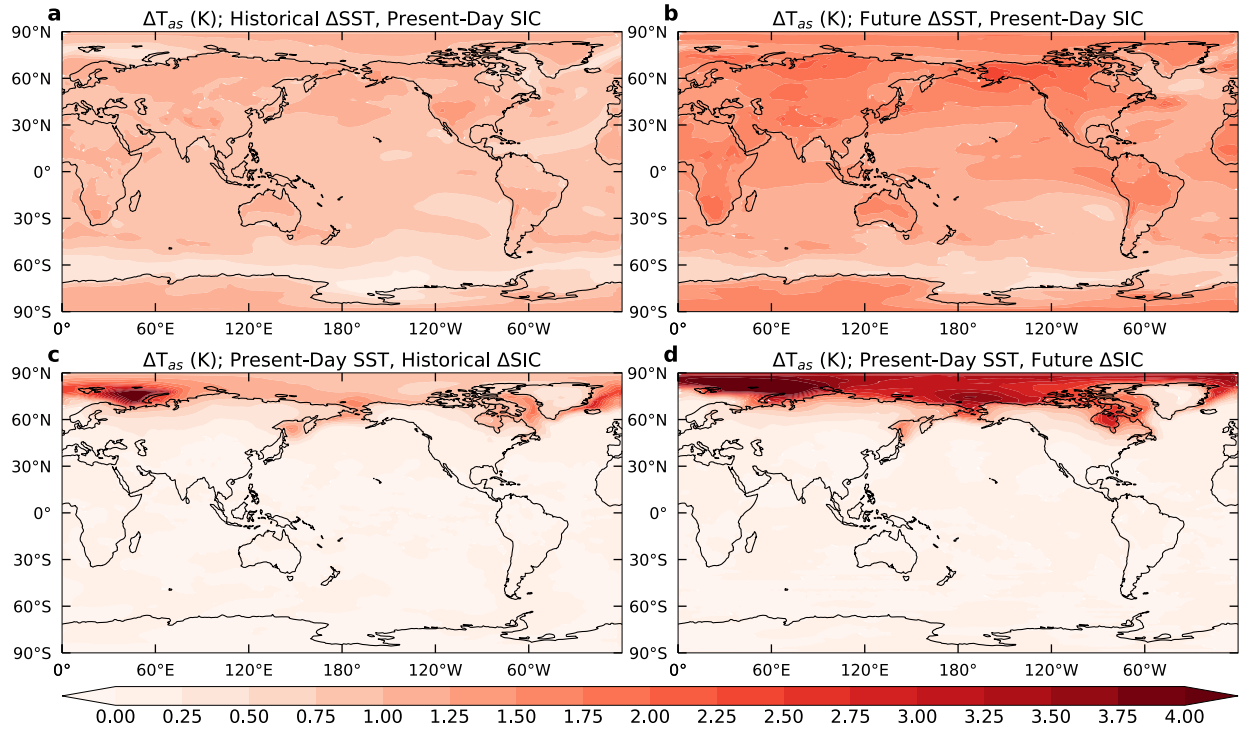
348 3. Results

349 3.1 Surface warming response to changes in global SST or Arctic SIC

350 We first examine the annual-mean surface air temperature response to historical and future
351 global SST (Fig. 2a, b) or Arctic SIC (Fig. 2c, d) changes shown in Figure 1. The globe experiences
352 relatively uniform warming in pdSST-pdSIC relative to piSST-pdSIC (Fig. 2a, referred to as
353 historical warming) and in futSST-pdSIC relative to pdSST-pdSIC (Fig. 2b, referred to as future
354 warming), with slightly greater magnitude in the future SST case than the historical case. Thus,
355 the SST perturbation runs show background global warming without noticeable AA. In contrast,

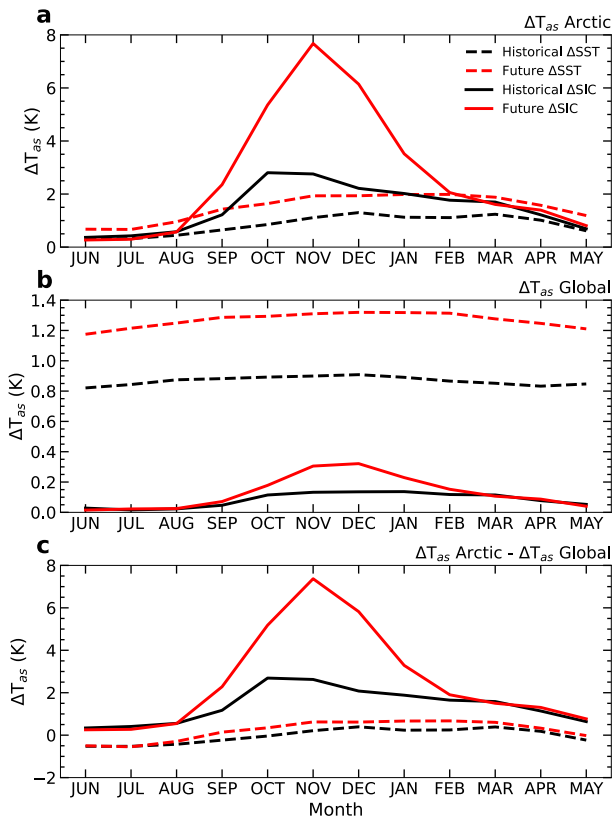
356 reduced Arctic sea-ice leads to large warming over Arctic oceanic areas with little temperature
357 change south of $\sim 60^\circ\text{N}$ and over northern high latitude land surfaces in both the historical and
358 future perturbed SIC runs (Fig. 2c, d). Note that the local Arctic warming is larger for the future
359 case than the historical case as the future sea-ice loss is larger (Fig. 1c, d) and that the largest
360 historical warming (Fig. 2c) occurs over the Barents-Kara Seas region where there is large sea-ice
361 loss (Fig. 1b).

362 The seasonal cycle of the surface air temperature changes averaged over the Arctic (Fig.
363 3a) and globe (Fig. 3b) shows different responses to global SST or Arctic SIC perturbations. Global
364 SST perturbations produce small Arctic warming during historical ($\sim 0.5\text{-}1.0\text{ K}$) and future ($\sim 1.0\text{-}$
365 2.0 K) periods for October-March and summer warming in the future global SST perturbation
366 simulation is larger than the future Arctic SIC experiment (Fig. 3a). The global-mean surface
367 temperature warms by $\sim 0.8\text{ K}$ for the historical and $\sim 1.2\text{ K}$ for the future SST cases, with little
368 seasonal variation (Fig. 3b). Thus, there is small AA during October-March while the summer
369 Arctic warming is weaker than the global-mean warming in the SST perturbation experiments
370 (Fig. 3c). In contrast, Arctic sea-ice loss produces large Arctic warming from October-January for
371 the historical and future cases, with weak warming in summer (Fig. 3a). Note that the peak
372 warming shifts from October in the historical case to November in the future case. The global-
373 mean warming response to the SIC changes is weak throughout most of the year except during late
374 autumn and early winter (Fig. 3b), which is due to the large warming in the Arctic (Fig. 2c-d). As
375 a result, AA is strong from October-January for the two perturbed SIC cases, especially for the
376 future SIC case (up to 7 K), while the AA is weak during the summer months (Fig. 3c).



377

378 **Fig. 2.** Multi-model ensemble mean changes in annual-mean surface air temperature (ΔT_{as}) in
 379 response to (a, c) historical and (b, d) future (a, b) SST and (c, d) SIC changes shown in Fig. 1.



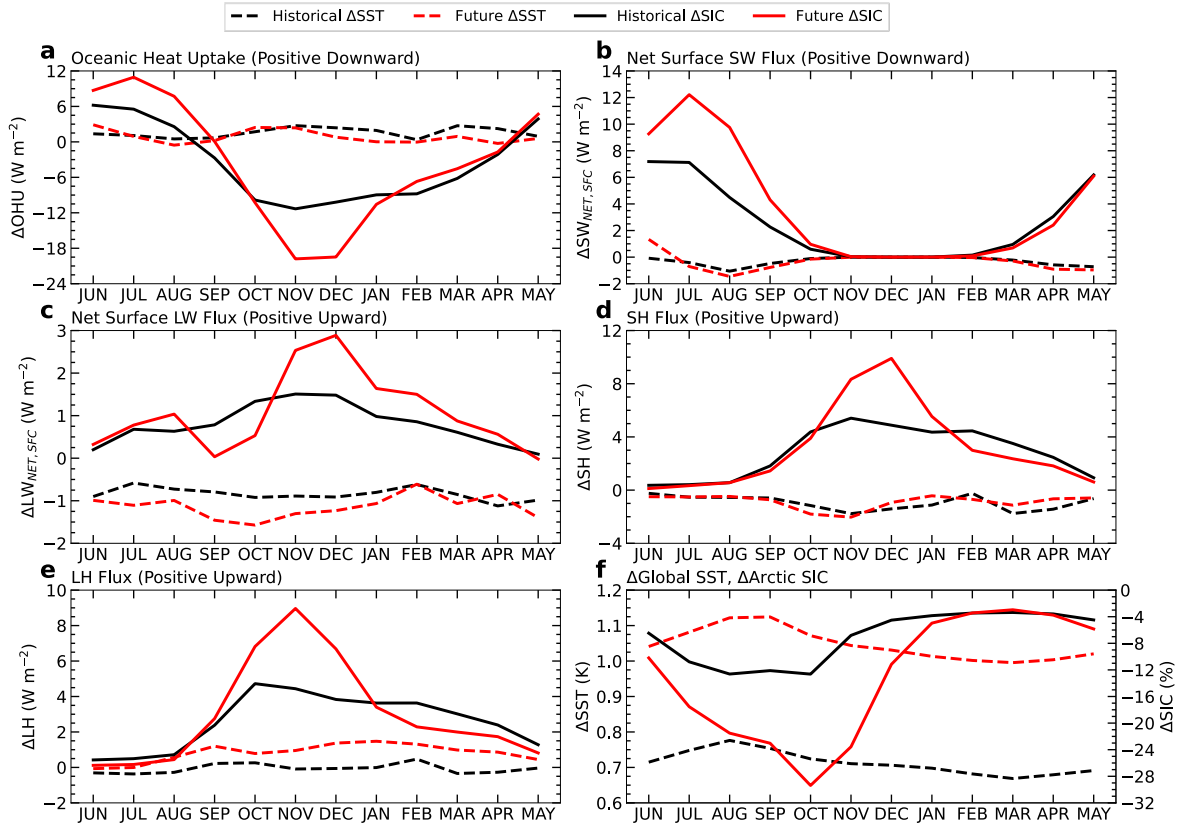
380

381 **Fig. 3.** Multi-model ensemble mean seasonal cycle of surface air temperature changes (ΔT_{as} ; in K)
382 in response to historical (black lines) and future (red lines) SST (dashed lines) and SIC (solid lines)
383 perturbations shown in Fig. 1 averaged over the (a) Arctic (67°-90°N) and (b) globe, and (c) Arctic
384 minus global-mean difference (i.e., Arctic amplification). Land surfaces are excluded in (a).
385

386 3.2 Surface energy budget response to Global SST or local Arctic SIC changes

387 Increased upward surface energy fluxes over sea-ice retreat areas have been shown to drive
388 large Arctic warming and AA in winter (Deser et al. 2010; Boeke and Taylor 2018; Taylor et al.
389 2018; Dai et al. 2019). In response to SST warming with fixed SIC, we find little change in the net
390 surface energy flux, net surface SW, SH, and LH fluxes over the Arctic Ocean throughout the year
391 (Fig. 4). The upward net surface LW flux decreases by $\sim 1 \text{ W m}^{-2}$ for both the historical and future
392 SST warming cases with fixed SIC (Fig. 4c). This represents a small increase in the downward
393 LW radiation, likely due to increased water vapor and enhanced atmospheric energy convergence
394 into the Arctic, rather than changes to surface conditions, as shown below. The suppressed Arctic
395 surface warming and weak oceanic energy flux response to SST warming without SIC changes is
396 consistent with Dai et al. (2019), who found similar results in model simulations with increasing
397 CO_2 concentrations and fixed Arctic sea-ice in flux calculations.

398 Arctic sea-ice loss greatly influences the magnitude and seasonal cycle of the Arctic
399 oceanic heat flux. From May-August, oceanic *absorption* of energy increases by $\sim 6\text{-}12 \text{ W m}^{-2}$ in
400 response to historical and future SIC loss (Fig. 4a) while during October-March oceanic *release*
401 of energy increases by $\sim 12\text{-}18 \text{ W m}^{-2}$ (Fig. 4a). Most of the increased oceanic energy absorption
402 from May-August is due to increased absorption of SW radiation (Fig. 4b), with negligible changes
403 in net surface LW, SH, and LH fluxes (Fig. 4c-e) during summer. In contrast, net surface LW, SH,
404 and LH fluxes are the main contributors to the enhanced cold-season oceanic energy release in
405 response to Arctic sea-ice loss (Fig. 4d, e). Further, the ocean surface emits more LW radiation to
406 the atmosphere from October-March for historical and future Arctic sea-ice loss runs (Fig. 4c).
407 The large increases in upward surface energy fluxes in response to sea-ice loss play an important
408 role in enhancing warming of the surface air and AA during winter (Fig. 3a).
409



410

411 **Fig. 4.** Arctic (67° - 90° N) multi-model ensemble mean seasonal cycle of changes in (a) OHU
 412 (positive downward), (b) net surface SW flux (positive downward), (c) net surface LW flux
 413 (positive upward), (d) SH flux (positive upward), and (e) LH flux (positive upward) in response
 414 to historical (black lines) and future (red lines) SST (dashed lines) and SIC (solid lines)
 415 perturbations shown in Fig. 1. All values are in W m^{-2} and land surfaces are excluded from
 416 averages. (f) The seasonal cycle of the historical (black lines) and future (red lines) global SST
 417 changes (left y-axis; dashed lines) and Arctic SIC loss (right y-axis; solid lines) specified in the
 418 SIC and SST perturbation experiments.

419

420 3.3 Feedback seasonal cycles and warming contributions

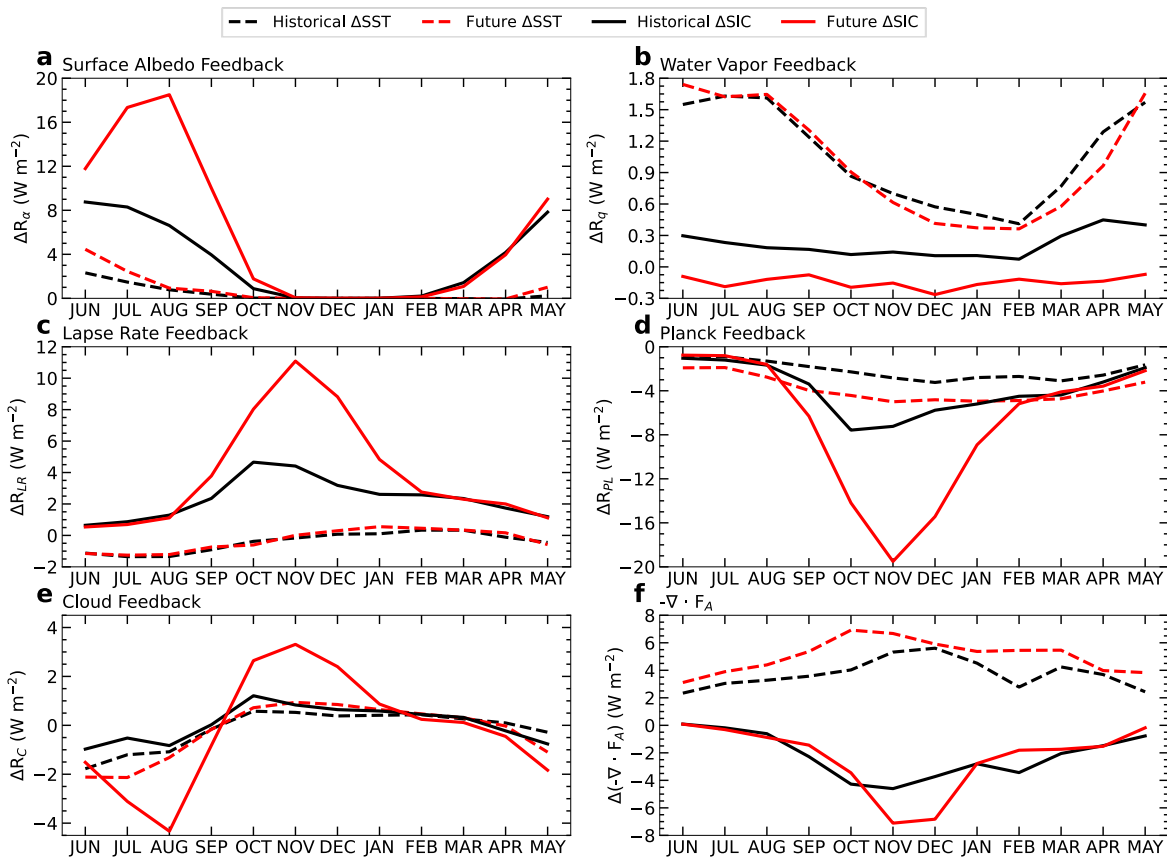
421 The contrasting surface warming responses to global SST changes or local sea-ice loss
 422 greatly influence Arctic climate feedbacks and atmospheric energy convergence changes. Figure
 423 5 shows the seasonal cycle of TOA radiative contributions of the climate feedbacks and
 424 atmospheric energy convergence; however, their corresponding climate feedback parameters (i.e.,
 425 the TOA radiative flux changes normalized the annual-mean Arctic surface warming) show similar
 426 seasonal cycles (not shown). Under global SST warming with fixed SIC, Arctic atmospheric
 427 energy convergence (Fig. 5f) and water vapor feedback (Fig. 5b) become important contributors

428 to the Arctic TOA flux change. Specifically, atmospheric energy convergence into the Arctic
429 responds similarly to historical and future SST warming, with increases of $\sim 4\text{-}7 \text{ W m}^{-2}$ during
430 October-March and $\sim 2\text{-}4 \text{ W m}^{-2}$ from April-September (Fig. 5f). This suggests that without
431 changes in sea ice, increased atmospheric energy transport becomes an important contributor to
432 small cold season Arctic warming and AA (Fig. 3). Further, the magnitude and seasonal cycle of
433 the water vapor feedback is similar between the historical and future SST cases, with maximum
434 water vapor feedback from May-August and minimum water vapor feedback during October-
435 March (Fig. 5b). This is expected as the warm-season Arctic would see larger water vapor
436 increases due to its warmer mean air temperatures. Arctic surface albedo (Fig. 5a), lapse rate (Fig.
437 5c), and Planck (Fig. 5d) feedbacks weakly respond to SST increases without sea-ice loss. Lastly,
438 we note that the net cloud feedback produces slight cooling in response to SST increases for June-
439 August (Fig. 5e).

440 In response to sea-ice loss, Arctic surface albedo feedback increases by $\sim 7\text{-}8 \text{ W m}^{-2}$ and
441 $\sim 12\text{-}18 \text{ W m}^{-2}$ for historical and future cases during the sunlit months (i.e., April-September) due
442 to increased exposure of dark water surfaces (Fig. 5a). The ocean, rather than the atmosphere,
443 absorbs much of the extra SW radiation (Fig. 4a), resulting in weak summer surface warming (Fig.
444 3a). Cloud feedback is negative in response to sea-ice loss during April-August, and the cooling is
445 larger in the future SIC case ($-1.5\text{-}4.5 \text{ W m}^{-2}$) than the preindustrial SIC run ($-1.0\text{-}1.5 \text{ W m}^{-2}$).
446 Lapse rate (Fig. 5c) and Planck (Fig. 5d) feedbacks weakly respond to historical or future Arctic
447 SIC changes in summer due to small surface warming (Fig. 3a) during the sunlit season. We also
448 find negligible water vapor feedback in response to Arctic sea-ice loss throughout the year, which
449 differs from the noticeable water vapor feedback in response to SST warming (Fig. 5b).

450 The large cold-season surface warming in response to historical and future Arctic sea-ice
451 loss enhances Arctic lapse rate (Fig. 5c) and Planck (Fig. 5d) feedbacks. When Arctic surface
452 warming (Fig. 3a) and AA (Fig. 3c) peak from October-December, the lapse rate feedback
453 increases the incoming TOA radiative flux by $\sim 4\text{-}6 \text{ W m}^{-2}$ ($\sim 8\text{-}11 \text{ W m}^{-2}$) and the Planck feedback
454 opposes warming by $-6\text{-}8 \text{ W m}^{-2}$ ($-16\text{-}20 \text{ W m}^{-2}$) due to historical (future) sea-ice loss. Note that
455 the month of maximum (minimum) lapse rate (Planck) feedback in the historical and future SIC
456 cases (Fig. 5c) corresponds to the month of peak Arctic surface warming (Fig. 3a), which in turn
457 is related to peak oceanic heating (Fig. 4a) induced by sea-ice loss (Fig. 4f) in these simulations.

458 The cloud feedback in response to future Arctic sea-ice loss also enhances the net incoming TOA
 459 radiative flux from October-January by $\sim 2.5\text{-}3.0 \text{ W m}^{-2}$, but the cloud feedback is weak ($<1.0 \text{ W}$
 460 m^{-2}) during winter in response to historical sea-ice loss (Fig. 5e). In contrast to the SST change
 461 simulations, Arctic atmospheric energy convergence weakens by $\sim 4 \text{ W m}^{-2}$ and $\sim 7 \text{ W m}^{-2}$ in
 462 response to historical and future sea-ice loss from November-December, respectively (Fig. 5f).
 463 Enhanced Arctic warming in response to sea-ice loss in the non-summer months (Fig. 3a) weakens
 464 the temperature gradient between the midlatitudes and polar regions, thus reducing atmospheric
 465 energy convergence into the Arctic region.

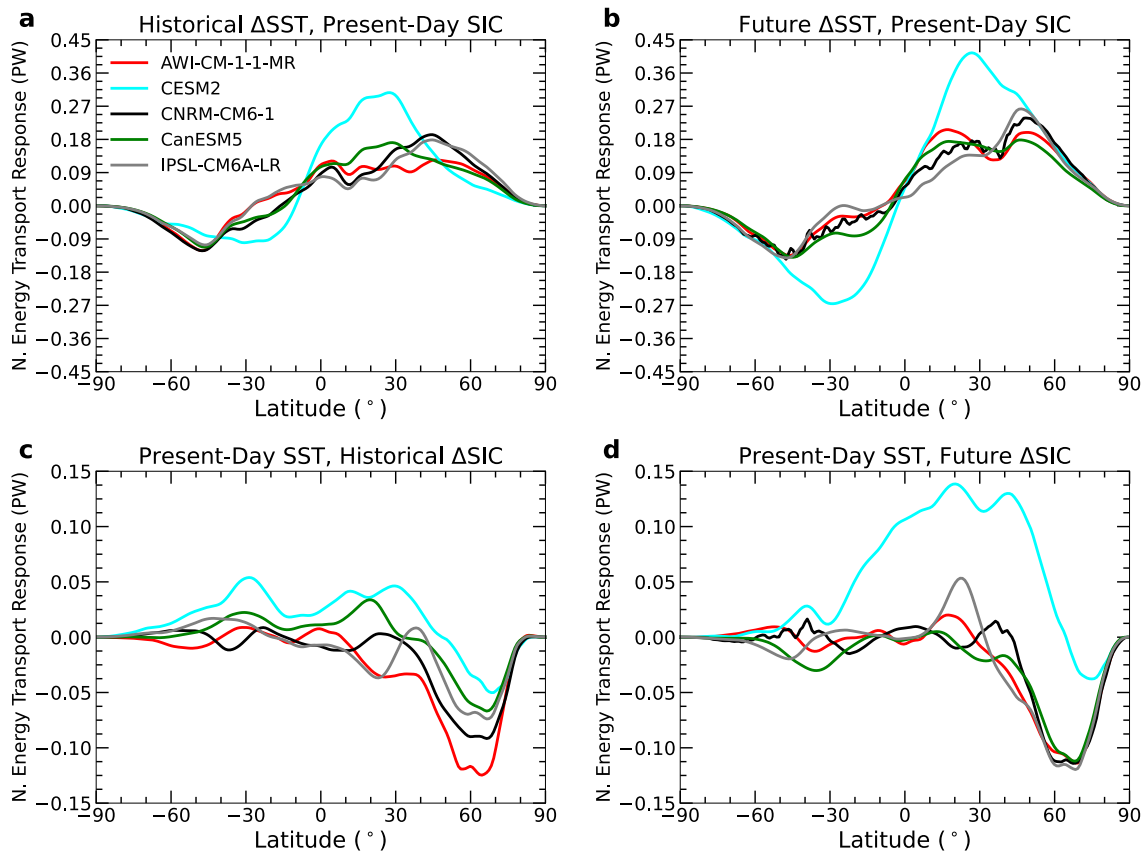


466

467 **Fig. 5.** Arctic ($67^{\circ}\text{-}90^{\circ}\text{N}$) multi-model ensemble mean seasonal cycle of the (a) surface albedo,
 468 (b) water vapor, (c) lapse rate, (d) Planck, and (e) cloud feedbacks, and (f) changes in atmospheric
 469 energy convergence into the Arctic in response to historical (black lines) and future (red lines) SST
 470 (dashed lines) and SIC (solid lines) changes shown in Fig. 1. All values are in W m^{-2} and land
 471 surfaces are excluded in averages except for the case shown in (f).
 472

473 Warmer SSTs enhance poleward atmospheric energy transport at all latitudes for each
 474 model for the historical (Fig. 6a) and future (Fig. 6b) SST warming cases, with slightly larger

475 increases in the northern hemisphere than southern hemisphere from October-March. All models, 476
 476 except CESM2, show enhanced cold season northward energy transport with peak increases of 477
 477 around $\sim 45^{\circ}$ - 50° N for the SST warming cases. In CESM2, atmospheric energy transport shows 478
 478 maximum increases around 30° N for October-March. Thus, without large Arctic warming related 479
 479 to sea-ice loss, the atmosphere displaces energy surpluses poleward. For the SIC perturbation 480
 480 experiments, there is a net decrease in poleward atmospheric energy transport around 30° - 90° N 481
 481 with a maximum decrease around 60° N but little change south of 30° N for both historical (Fig. 482
 482 6c) and future (Fig. 6d) sea-ice loss, consistent with previous studies (Deser et al. 2015; Audette 483
 483 et al. 2021). Again, CESM2 is an outlier compared to the rest of the models for the future Δ SIC 484
 484 run as northward atmospheric energy transport increases from 30° - 60° N (Fig. 6d) for this model. 485
 485 Therefore, SST-induced background warming enhances atmospheric poleward energy transport 486
 486 into the polar regions, while large Arctic warming in response to sea-ice loss weakens atmospheric 487
 487 poleward energy transport over the northern mid-high latitudes.



488

489 **Fig. 6.** Changes in October-March mean northward energy transport in response to (a, c) historical
 490 and (b, d) future (a, b) SST and (c, d) SIC changes shown in Fig. 1.

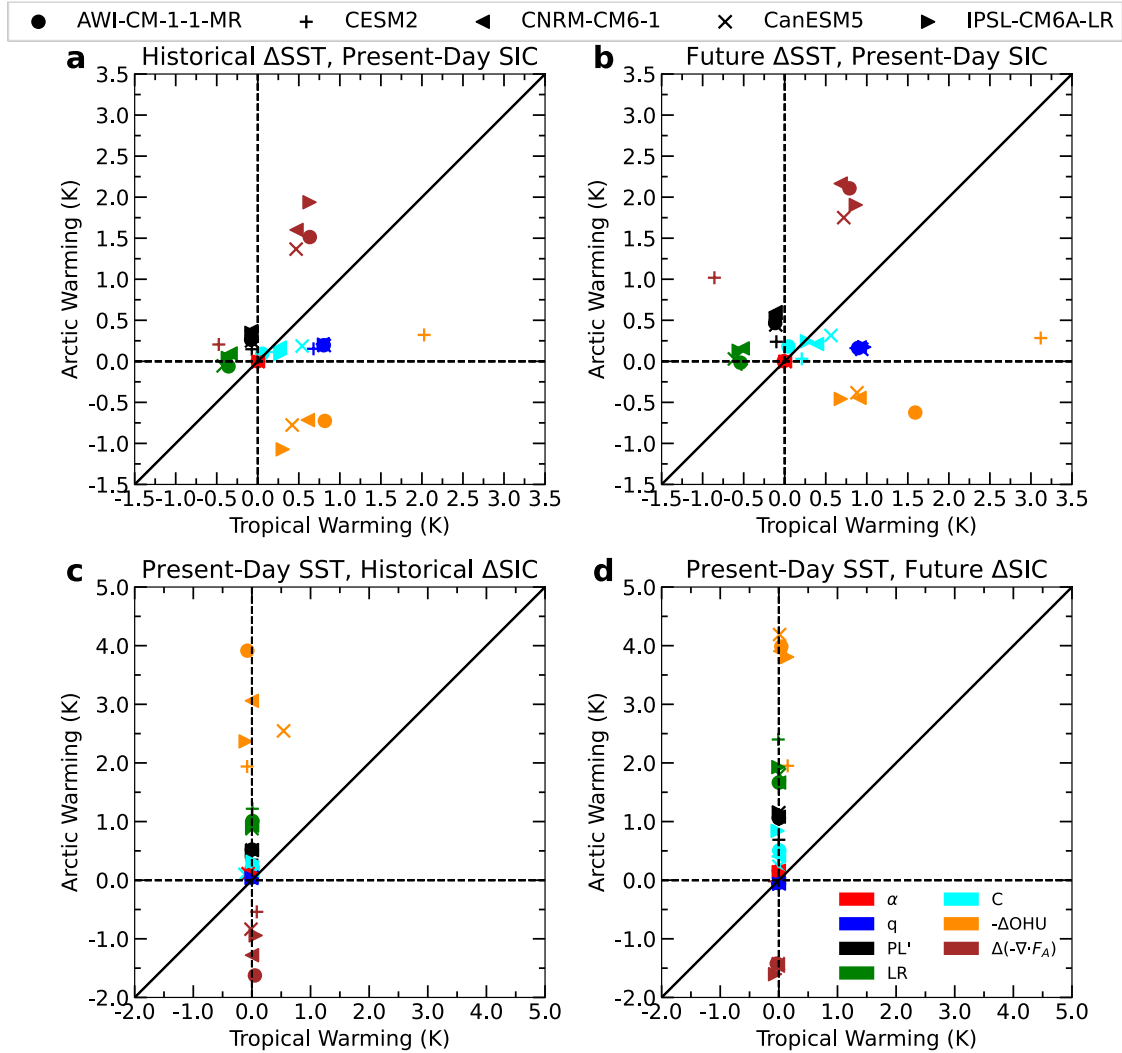
491

492 Figure 7 shows the *potential* warming contributions of the climate feedbacks over the
493 Arctic and the tropics for October-March as AA is largest in autumn and winter. We recognize
494 that warm season feedbacks in fully-coupled climate models indirectly affect Arctic surface
495 warming in winter by increasing summer oceanic energy storage that is later released to the
496 atmosphere in the cold season (Dai 2021). However, the delayed winter oceanic heat release due
497 to increased summer oceanic heat storage is absent in atmosphere-only simulations with specified
498 SST and SIC. Atmospheric energy convergence is the largest contributor for October-March (Fig.
499 7a, b) Arctic warming under historical (Fig. 7a) and future (Fig. 7b) global SST changes, as it
500 redistributes the energy from the lower latitude oceans, where SSTs increase, to the Arctic region.
501 In contrast, oceanic heat release opposes AA in response to global SST warming for October-
502 March (Fig. 7a, b) because the warmer SSTs produce a greater ocean-to-atmosphere energy flux
503 outside the Arctic, thus causing more warming in the tropics than in the Arctic. We note that the
504 warming contribution of $-\Delta\text{OHU}$ in the tropics and cooling effect of $-\Delta\text{OHU}$ in the Arctic may be
505 related to reduced poleward oceanic heat transport that is implicitly included in the historical and
506 future SST fields. However, analyses of simulations with a coupled atmosphere-ocean are needed
507 to confirm the role of oceanic heat transport on Arctic and tropical warming. Water vapor feedback
508 makes a small contribution to Arctic warming due to low October-March mean temperatures but
509 contributes to ~ 1 K of warming in the tropics in response to global SST warming (Fig. 7b),
510 opposing AA. Without sea-ice loss, lapse rate feedback contributes little to Arctic warming but
511 produces weak tropical cooling in response to historical (Fig. 7a) and future (Fig. 7b) SST
512 increases for the cold season. The local Planck feedback (relative to the global-mean Planck
513 feedback) slightly contributes to AA in the SST warming runs because the cooling effects from
514 Planck feedback are slightly less in the Arctic region than over the rest of the world (Fig. 7).
515 Surface albedo feedback contributes to negligible Arctic warming or AA from October-March in
516 response to global SST increases and fixed Arctic SIC during for historical (Fig. 7a) and future
517 (Fig. 7b) cases.

518 In response to Arctic sea-ice loss with fixed global SSTs, oceanic heat release is the largest
519 contributor to AA from October-March in historical (Fig. 7c) and future (Fig. 7d) SIC cases,
520 followed by the positive lapse rate feedback. This supports previous studies that showed that sea-

521 ice loss and oceanic energy release during Arctic winter are necessary to trigger large surface
522 warming and thus strong positive lapse rate feedback in the Arctic (Feldl et al. 2020; Jenkins and
523 Dai 2021; Dai and Jenkins 2023). The local Planck feedback (relative to the global-mean Planck
524 feedback) also contributes to Arctic warming and AA in response to historical (Fig. 7c) and future
525 (Fig. 7d) Arctic SIC changes by cooling the Arctic region less than the tropics. Additionally,
526 positive cloud feedback makes a slight contribution to cold-season Arctic warming and AA in
527 response to future Arctic SIC loss (Fig. 7d), but the contribution is negligible in the historical SIC
528 loss run (Fig. 7c). Water vapor feedback is suppressed over the Arctic and globe in the historical
529 (Fig. 7c) and future (Fig. 7d) SIC runs, suggesting that local sea-ice loss and water vapor feedback
530 are decoupled, as found previously (Jenkins and Dai 2021). In contrast to the perturbed SST runs,
531 the atmosphere displaces energy away from the Arctic in response to cold season sea-ice loss (Fig.
532 7c,d), thus opposing AA.

533 Note that warming contributions from changes in oceanic heat release ($-\Delta\text{OHU}$) and
534 changes in Arctic atmospheric energy convergence in response to historical (Fig. 7a) and future
535 (Fig. 7b) SST warming in CESM2 differ from the other models during October-March.
536 Specifically, CESM2 oceanic heat release slightly contributes to Arctic warming whereas in the
537 other models, oceanic heat release contributes to Arctic cooling. Due to the warming effect of the
538 $-\Delta\text{OHU}$ term in response to SST changes in CESM2, Arctic atmospheric energy convergence
539 weakens and does not need to compensate the cooling effect of $-\Delta\text{OHU}$ as in the other models
540 (Fig. 7a, b). Further, CESM2 $-\Delta\text{OHU}$ makes a weaker positive contribution to AA during October-
541 March in response to historical (Fig. 7c) and future (Fig. 7d) Arctic SIC. Atmospheric energy
542 convergence thus opposes AA less in CESM2 than the other models as $-\Delta\text{OHU}$ produces less
543 Arctic cooling in CESM2 than the other models. We realize that more work is needed to validate
544 these statements.



545

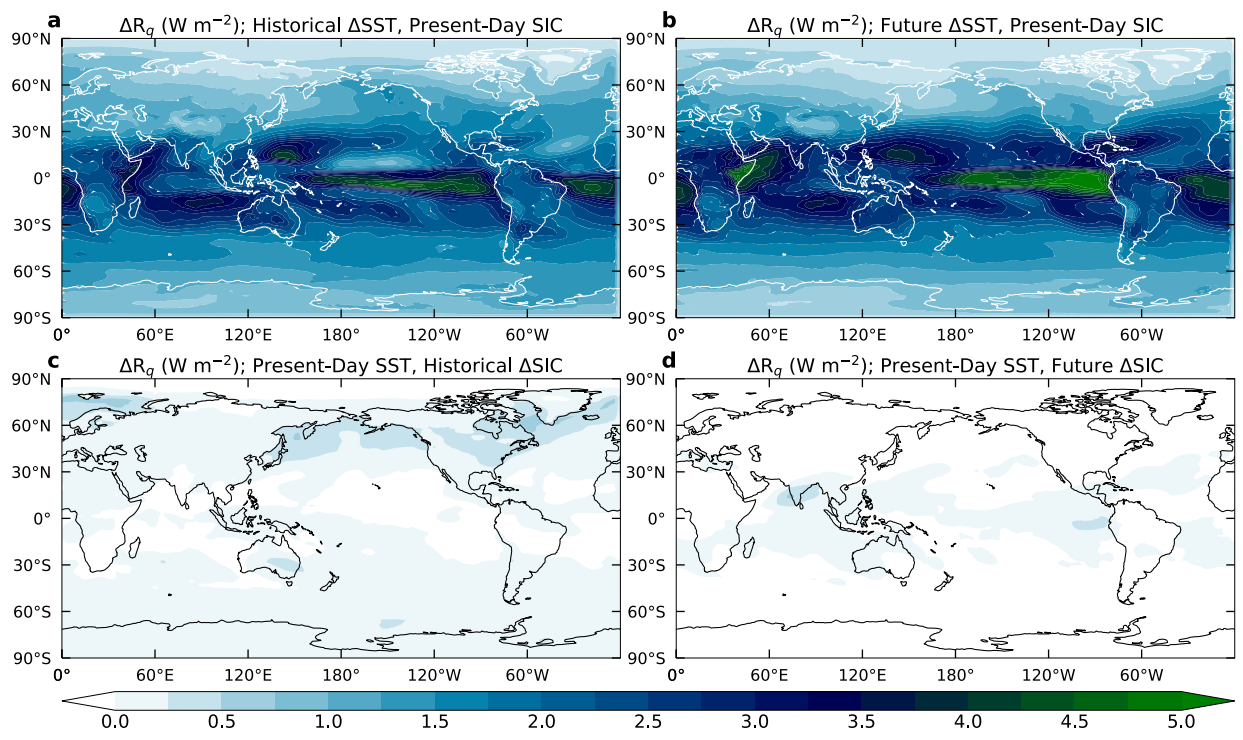
546 **Fig. 7.** Inter-model spread in ensemble mean, October-March *potential* warming contributions (in
 547 K) of Arctic (67°-90°N) vs. tropical (23.5°S-23.5°N) surface albedo (α), water vapor (q), Planck
 548 (PL'), lapse rate (LR), and cloud (C) feedbacks, and changes in oceanic heat release ($-\Delta\text{OHU}$;
 549 positive upwards), and atmospheric energy convergence ($\Delta(-\nabla \cdot \mathbf{F}_A)$) in response to (a, c)
 550 historical and (b, d) future (a, b) SST and (c, d) SIC perturbations shown in Fig. 1.

551

552 3.4 Physical processes underlying climate feedbacks

553 Water vapor feedback is complicated in high latitudes due to local temperature inversions
 554 and low amounts of water vapor (Curry et al. 1995; Sejas et al. 2018). Global maps reveal that
 555 SST warming (Fig. 8a, b) has a larger effect than local sea-ice loss (Fig. 8c, d) on water vapor
 556 feedback in both the Arctic and the rest of the globe. Specifically, water vapor feedback is largest

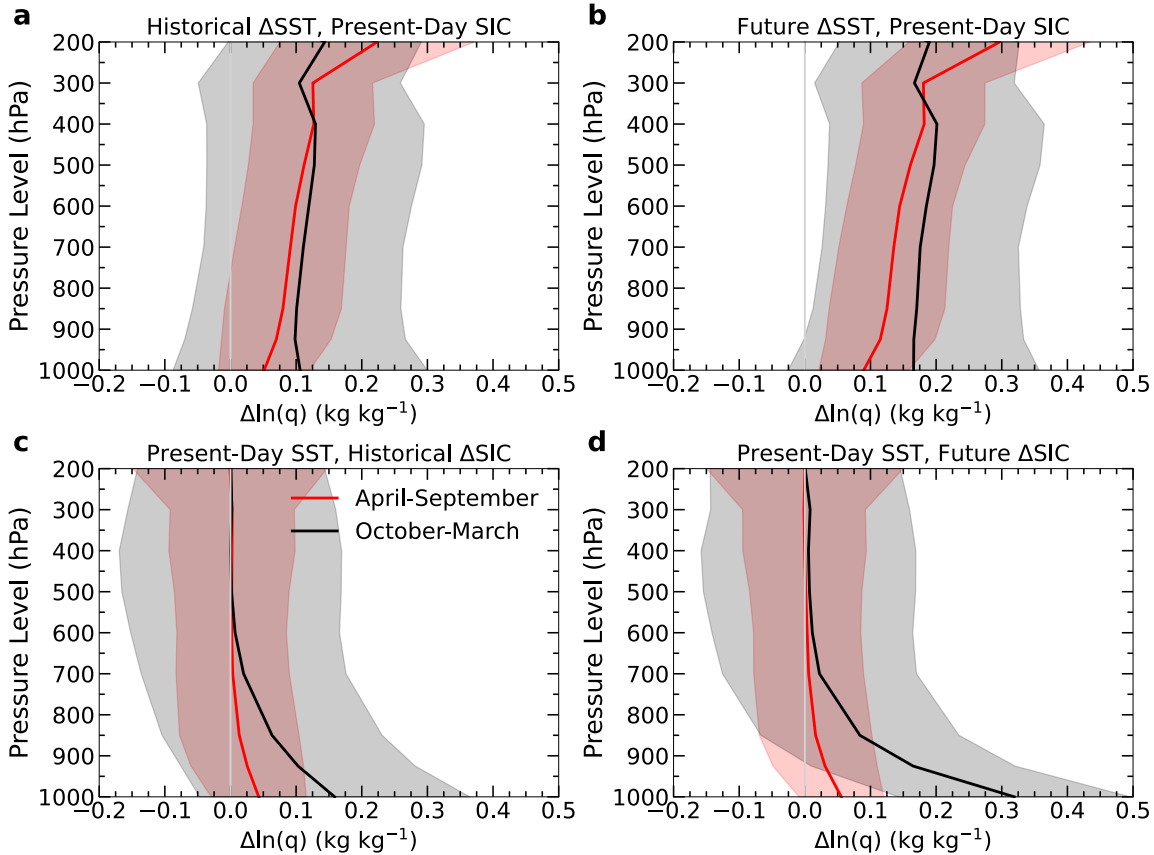
557 near the equator at $\sim 2\text{-}5 \text{ W m}^{-2}$ in response to historical (Fig. 8a) and future (Fig. 8b) SST warming
 558 and decreases poleward to $\sim 0.5\text{-}1.0 \text{ W m}^{-2}$ in the Arctic region (Fig. 8a, b). The cold-season water
 559 vapor feedback is weak in response to Arctic sea-ice loss (Fig. 8c, d), including over the Arctic
 560 where low-level specific humidity increases (Fig. 9c, d). This is due to low or negative values of
 561 the October-March LW and net (i.e., LW+SW) water vapor kernel in the Arctic lower troposphere
 562 (Fig. 10a, c). Because the water vapor feedback is most sensitive to upper tropospheric water vapor
 563 content (Shell et al. 2008; Soden et al. 2008; Pendergrass et al. 2018), the low-level water vapor
 564 increases in response to Arctic sea-ice loss do not lead to large TOA flux changes.



565
 566 **Fig. 8.** Multi-model ensemble mean October-March water vapor feedback (in W m^{-2}) in response
 567 to (a, c) historical and (b, d) future (a, b) SST and (c, d) SIC changes shown in Fig. 1.
 568

569 Slight positive water vapor feedback occurs over sea-ice loss areas in the historical SIC
 570 loss run ($\sim 0.50\text{-}0.75 \text{ W m}^{-2}$; Fig. 8c) but there are negligible water vapor feedback effects in the
 571 Arctic under future SIC conditions (Fig. 8d). As the October-March LW and net water vapor kernel
 572 is negative near the surface (Fig. 10a, c) due to temperature inversions in the Arctic (Shell et al.
 573 2008; Soden et al. 2008), any increase in moisture in the lower troposphere will result in enhanced
 574 radiative emission to space (i.e., a negative water vapor radiative effect). In response to future
 575 Arctic SIC (Fig. 9d), there are greater increases in the natural logarithm of specific humidity

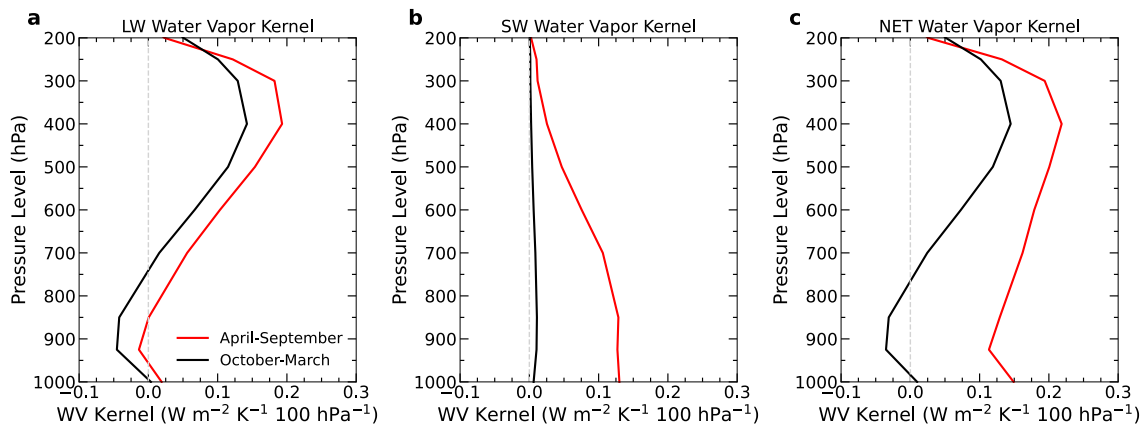
576 [$\Delta\ln(q)$] in the lower troposphere than in the historical case (Fig. 9c). Thus, greater future lower
577 tropospheric moistening in the Arctic region produces a more negative water vapor radiative effect
578 at the TOA. We also note that there is a large spread (as shown by the standard deviation) among
579 the PAMIP models and individual ensemble members in upper tropospheric moistening in the
580 perturbed Arctic SIC runs, where there is little change in the mean $\Delta\ln(q)$ (Fig. 9c, d). Thus, some
581 ensemble members may have experienced a slight decrease in upper tropospheric $\Delta\ln(q)$ in
582 response to Arctic sea-ice loss with fixed global SST, enhancing outgoing LW radiation at the
583 TOA. In contrast, the historical (Fig. 10a) and future (Fig. 10b) perturbed SST runs experienced
584 slightly greater $\Delta\ln(q)$ in the upper troposphere than the lower troposphere for both warm and cold
585 seasons. Due to positive values of the TOA LW and net Arctic water vapor kernel in the upper
586 troposphere (Fig. 10a, c), top-heavy moistening in response to global SST warming produces a
587 positive water vapor feedback from the TOA perspective. We note that the vertical structure of
588 $\Delta\ln(q)$ is greater at each level for April-September in the perturbed SST runs than the changed
589 Arctic SIC simulations. Thus, the vertical moistening profile, in addition to the vertical structure
590 of the water vapor kernel, plays a role for the Arctic summer water vapor feedback in the perturbed
591 SST experiments with fixed Arctic SIC.



592

593 **Fig. 9.** Multi-model, ensemble mean (solid lines) Arctic (67° - 90° N; land surfaces excluded)
 594 changes in the natural logarithm of specific humidity (in kg kg^{-1} ; solid lines) in response to (a, c)
 595 historical and (b, d) future (a, b) global SST and (c, d) Arctic SIC changes shown in Fig. 1. The
 596 shading shows ± 1 standard deviation from the multi-model ensemble mean profile.

597

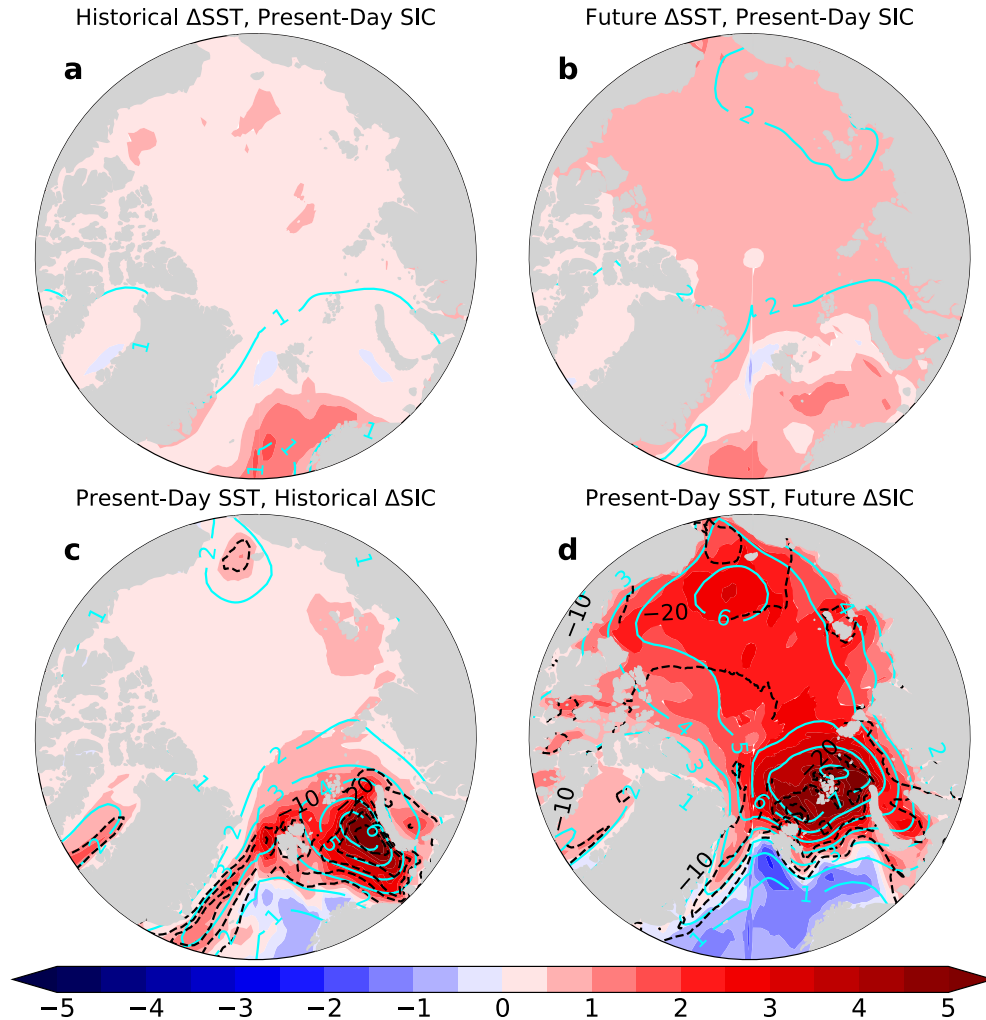


598

599 **Fig. 10.** Profiles of the Pendergrass et al. (2018) TOA (a) LW, (b) SW, and (c) NET (LW+SW)
 600 water vapor kernel (in $\text{W m}^{-2} \text{K}^{-1} 100 \text{hPa}^{-1}$) averaged over the Arctic region (67° - 90° N).

601

602 Arctic low cloud amount has been suggested to increase during the cold season in response
603 to sea-ice loss due to decreased lower tropospheric stability (Kay and Gettelman 2009; Jenkins et
604 al. 2023), thus affecting Arctic cloud feedback (Vavrus 2004; Morrison et al. 2019; Jenkins and
605 Dai 2022). We find weak October-March cloud feedback in response to perturbed SST with fixed
606 Arctic SIC for historical (Fig. 11a) and future (Fig. 11b) cases, suggesting that remote processes
607 do not greatly impact Arctic cloud feedback in the cold season. On the other hand, Arctic sea-ice
608 loss produces a large positive cloud feedback response in winter, especially in regions with large
609 sea-ice loss and surface warming (Fig. 11c, d). For the run with historical SIC loss, cloud feedback
610 enhances the TOA radiative flux by $\sim 2\text{-}5 \text{ W m}^{-2}$ in the Barents-Kara Seas region and by $\sim 0.5\text{-}1.0$
611 W m^{-2} in the Chukchi Sea, where the largest sea-ice loss and surface warming occurs. Under future
612 Arctic sea-ice loss, cold-season cloud feedback is largest in the Barents-Kara Seas ($\sim 3\text{-}5 \text{ W m}^{-2}$)
613 except the warming effects from clouds extend into the Central Arctic Ocean. This is likely related
614 to the greater area with large sea-ice loss (Fig. 1b, d) and surface warming (Fig. 2c-d) in the future
615 case than in the historical case.



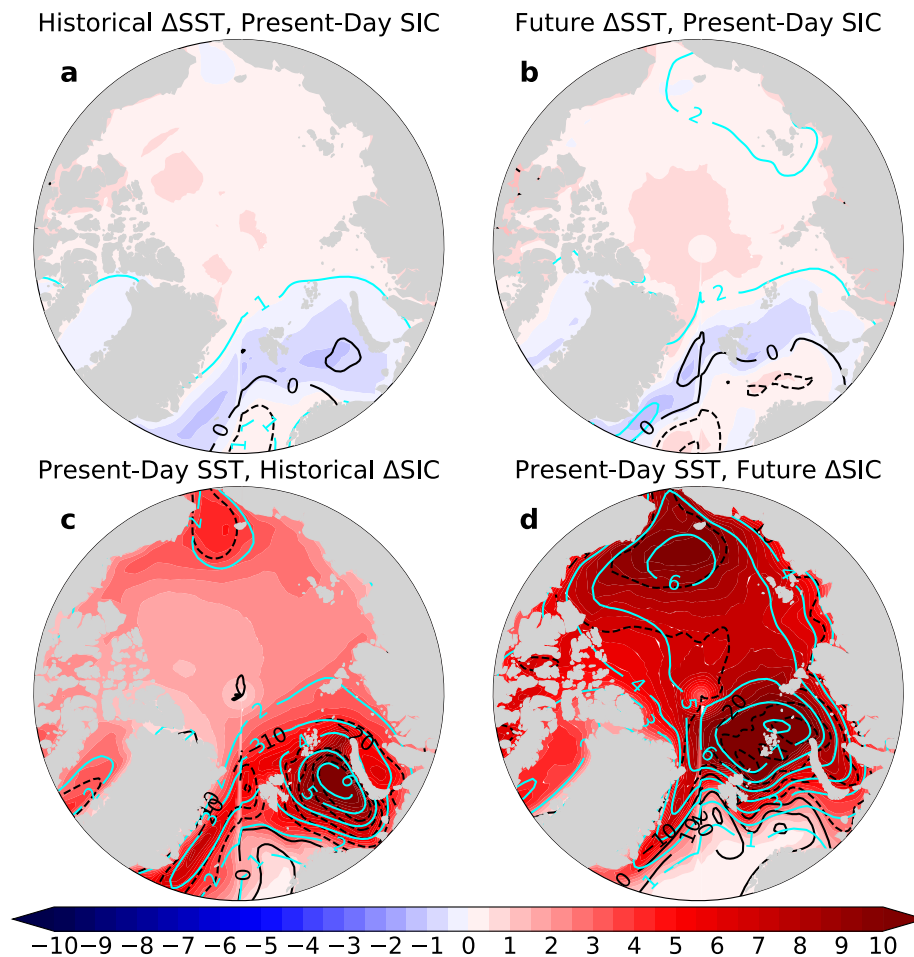
616

617 **Fig. 11.** Multi-model ensemble mean TOA radiative flux change due to the cloud feedback
 618 (shading; in $W m^{-2}$) and change in surface air temperature (cyan contours; in K) averaged over
 619 October-March in response to (a, c) historical and (b, d) future (a, b) SST and (c, d) SIC changes.
 620 Black contours in (c) and (d) show the change in Arctic SIC for October-March.

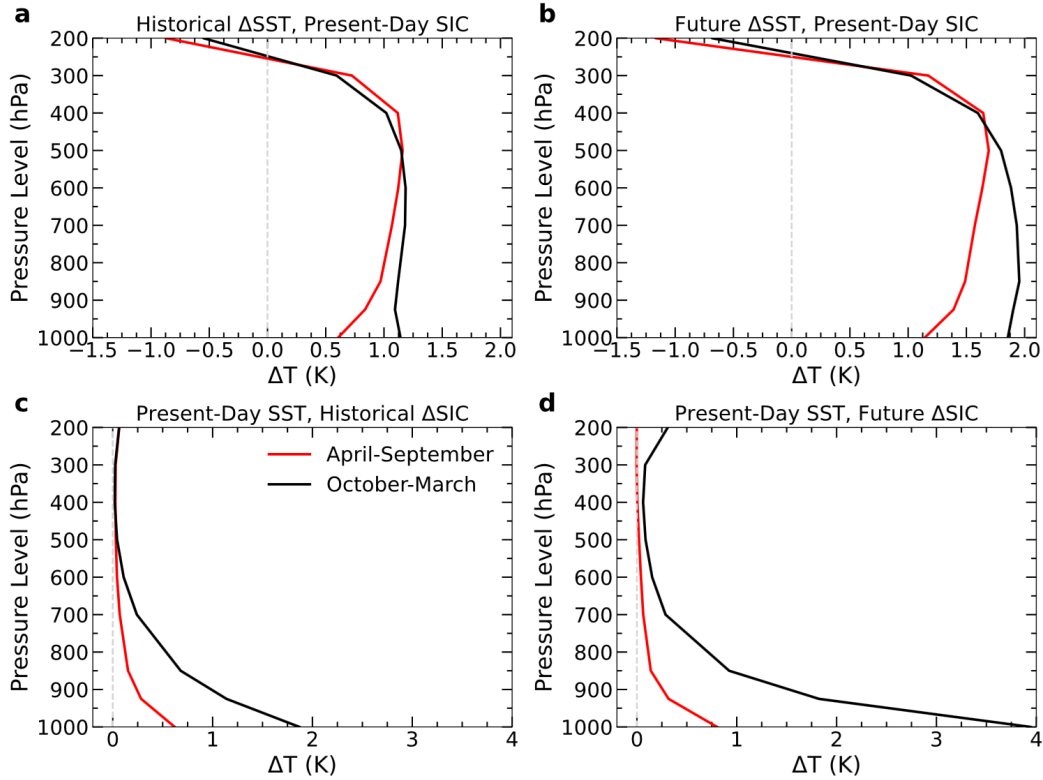
621

622 The lapse rate feedback experiences large seasonal and spatial variations in the Arctic in
 623 response to SST warming or Arctic SIC loss. From October-March, the lapse rate feedback is
 624 negative-neutral in response to the global SST warming (Fig. 12a, b) due to relatively uniform
 625 vertical warming profiles (Fig. 13a, b). We note that without changes in SIC, there are negligible
 626 changes in Arctic oceanic heat uptake or surface warming in the cold season, leading to suppressed
 627 lapse rate feedback (Fig. 12a, b). In contrast, cold-season sea-ice loss enhances Arctic lapse rate
 628 feedback for historical (Fig. 12c) and future (Fig. 12d) SIC cases when surface and lower

629 tropospheric warming outpaces warming in the mid-upper troposphere (Fig. 13c, d). We note that
 630 lapse rate feedback strengthens ($\sim 6\text{-}10\text{ W m}^{-2}$) in regions with the greatest October-March oceanic
 631 heat release and surface warming in response to historical (Fig. 12c) and future (Fig. 12d) sea-ice
 632 loss, consistent with previous studies (Dai et al. 2019; Feldl et al. 2020; Boeke et al. 2021; Jenkins
 633 and Dai 2021, 2022; Dai and Jenkins 2023). Thus, sea-ice loss is necessary to produce bottom-
 634 heavy warming and trigger Arctic positive lapse rate feedback during winter, as shown previously
 635 by Dai and Jenkins (2023) using coupled model experiments.



636
 637 **Fig. 12.** Multi-model, ensemble mean TOA radiative flux change due to the lapse rate feedback
 638 (shading; in W m^{-2}), changes in oceanic heat uptake (black contours; in W m^{-2} ; positive
 639 downward), and changes in surface air temperature (cyan contours; in K) averaged over October-
 640 March in response to (a, c) historical and (b, d) future (a, b) SST and (c, d) SIC changes.
 641



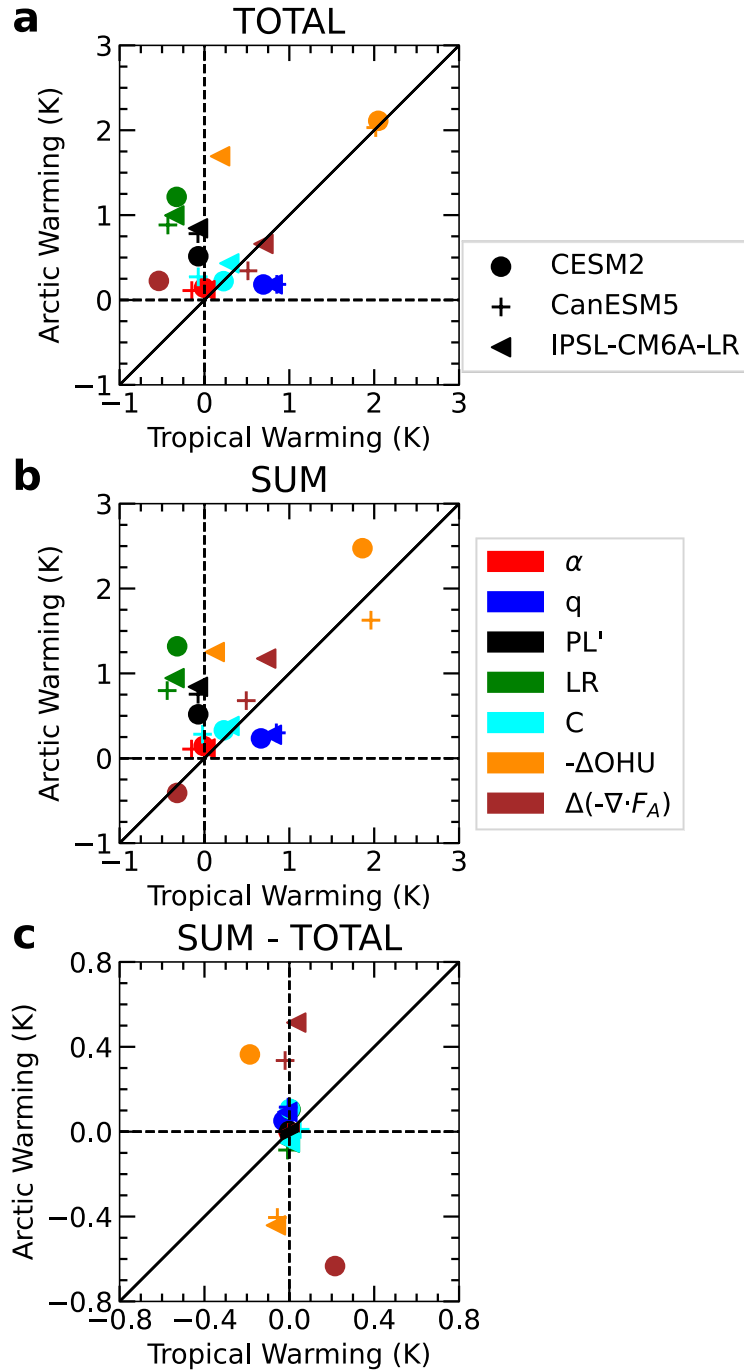
642
643
644
645
646
647

Fig. 13. Multi-model, ensemble mean Arctic (67° - 90° N; land surfaces excluded) temperature change profiles (in K) averaged over April-September (red lines) and October-March (black lines) in response to the (a) historical and (b) future global SST warming, and (c) historical and (d) future Arctic sea-ice loss.

648 3.5 Response to simultaneous SST and SIC changes

649 We compare the Arctic vs. tropical October-March potential warming contributions of
650 climate feedbacks, changes in atmospheric energy convergence and oceanic heat release in
651 response to historical global SST warming and historical polar sea-ice loss together (i.e., pdSST-
652 pdSIC minus piSST-piSIC; Fig. 14a; referred to as TOTAL) and the sum of the separate responses
653 to historical SST warming (i.e., pdSST-pdSIC minus piSST-pdSIC) and historical polar sea-ice
654 loss (i.e., pdSST-pdSIC minus pdSST-piArcSIC and pdSST-piAntSIC) (Fig. 14b; referred to as
655 SUM). The warming contributions of the lapse rate, water vapor, cloud, and Planck feedbacks in
656 TOTAL match SUM well, with the lapse rate feedbacks making the largest contribution to AA
657 (Fig. 14). Except for CESM2 in TOTAL, the change in atmospheric energy convergence makes
658 roughly equal warming contributions to Arctic and tropical warming from October-March,
659 suggesting that remote SST warming and Arctic sea-ice loss have opposing effects on the

660 horizontal atmospheric energy flux. The oceanic heat release changes in IPSL-CM6A-LR makes
661 a greater contribution to Arctic than tropical warming, but there are slight discrepancies between
662 CanESM5 and CESM2 oceanic heat release between TOTAL and SUM. In TOTAL, CanESM5
663 and CESM2 oceanic heat release changes contributes roughly the same amount to Arctic and
664 tropical warming; however, CESM2 (CanESM5) produces slightly greater Arctic (tropical)
665 warming in SUM. The surface albedo feedback is inactive from October-March due to lack of
666 sunlight and is not a major direct contributor to large cold-season AA. The differences between
667 feedbacks calculated with TOTAL and SUM are small except for oceanic heat release and
668 atmospheric energy convergence changes, where there are slight differences in their Arctic vs.
669 tropical warming contributions (Fig. 14c).

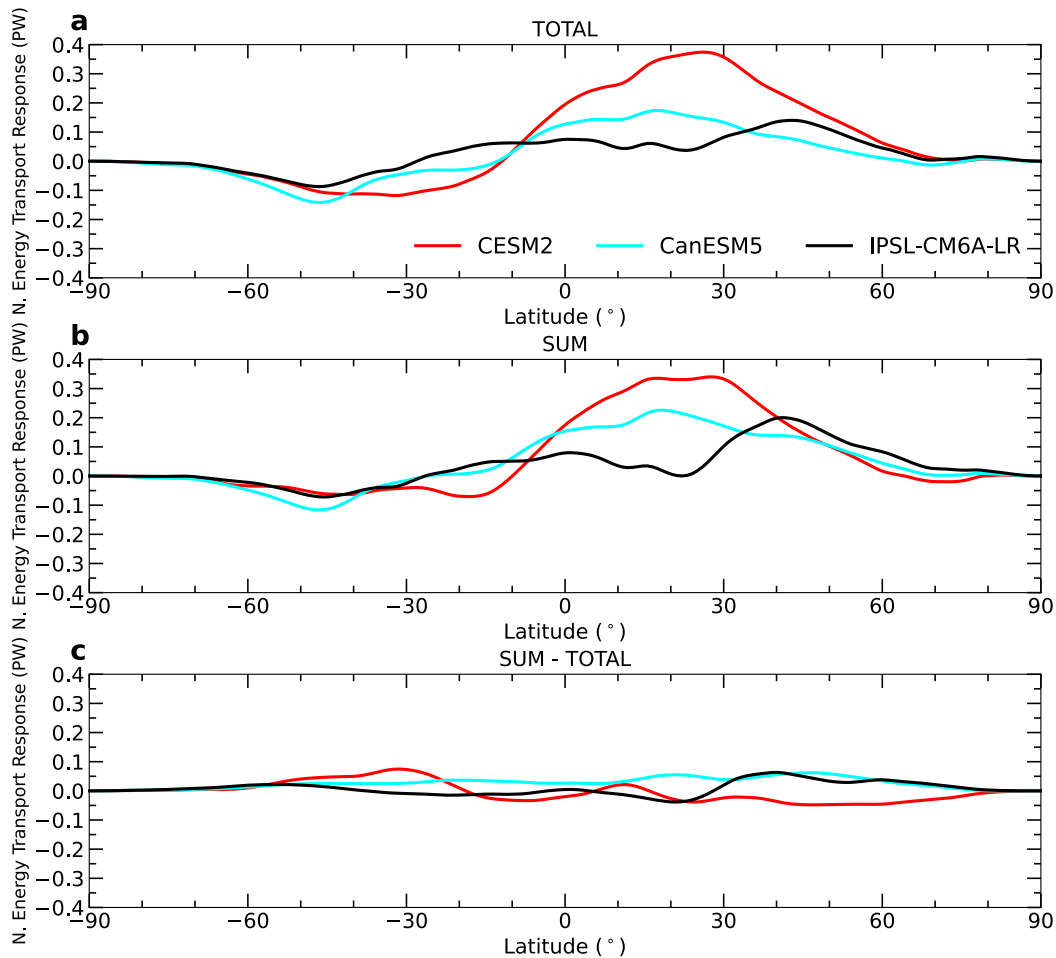


670

671 **Fig. 14.** Inter-model spread in the ensemble mean October-March *potential* warming contributions
 672 (in K) for Arctic ($67^\circ\text{-}90^\circ\text{N}$) and tropical ($23.5^\circ\text{S}\text{-}23.5^\circ\text{N}$) surface albedo (α), water vapor (q),
 673 Planck (PL'), lapse rate (LR), and cloud (C) feedbacks, and changes in oceanic heat release ($-\Delta\text{OHU}$;
 674 ΔOHU ; positive upwards) and atmospheric energy convergence ($\Delta(-\nabla \cdot F_A)$) in response to
 675 historical changes in global SST and polar SIC for (a) TOTAL (i.e., global SST and polar SIC
 676 change together), (b) SUM (i.e., sum of the response to the SST and SIC change separately), and
 677 (c) difference between (b) and (a).

678

679 The northward atmospheric energy transport response to the SST and SIC perturbations is
680 similar among TOTAL (Fig. 15a) and SUM (Fig. 15b), with little difference between the two cases
681 (Fig. 15c). In the tropical regions (i.e., 30°S-30°N), global SST warming enhances poleward
682 atmospheric energy transport by ~0.1-0.15 PW in the southern hemisphere and ~0.1-0.35 PW in
683 the northern hemisphere. Around 60°-90°N, there is little net change in atmospheric energy
684 transport in response to simultaneous SST and SIC changes, suggesting that remote warming due
685 to SST changes and local Arctic warming related to sea-ice loss have opposing effects on Arctic
686 atmospheric energy transport (Fig. 6a, c). The similarity of climate feedbacks (Fig. 14) and the
687 atmospheric energy transport (Fig. 15) response between TOTAL and SUM suggest that the effects
688 of SIC or SST changes can be linearly separated. In other words, the individual responses to SST
689 or SIC perturbations approximately sum to the combined influence of changes in SST and SIC.



690

691 **Fig. 15.** October-March northward energy transport response (in PW) in response to historical
692 changes in SST and SIC for (a) TOTAL and (b) SUM, and (c) difference between (b) and (a).

693

694 **4. Summary and Conclusions**

695 We investigated the impacts of historical and future Arctic sea-ice loss and global SST
696 increases on Arctic climate feedbacks, atmospheric energy convergence into the Arctic, and
697 oceanic heat release using PAMIP atmosphere-only simulations. The SST increase with fixed polar
698 sea ice results in relatively uniform global warming with negligible AA for both historical and
699 future cases. In contrast, historical and future Arctic sea-ice loss leads to large Arctic warming
700 with negligible effects south of $\sim 60^\circ\text{N}$, although this may not be the case in fully coupled
701 simulations (Deser et al. 2015). The PAMIP experiments allowed us to separate the response of
702 Arctic climate feedbacks, atmospheric energy convergence, and oceanic heat release to
703 background global warming without AA (as in the SST perturbation runs) or to large AA with
704 negligible warming outside the Arctic (as in the SIC change runs). We also found striking
705 similarities between the historical simulations with both SST and SIC changes together (i.e.,
706 TOTAL), and the sum of the individual responses to the historical SST and polar SIC changes (i.e.,
707 SUM) in terms of Arctic climate feedbacks and atmospheric energy transport response.

708 Under warmer global SSTs without sea-ice loss, Arctic winter oceanic heat release is
709 suppressed leading to weak Arctic cold season warming. Instead, enhanced poleward atmospheric
710 energy convergence rather than increased oceanic heat release becomes the dominant contributor
711 to *small* AA in response to global SST increases with fixed Arctic sea-ice. We also found strong
712 global water vapor feedback in the historical and future SST warming runs, especially in the
713 tropics. Water vapor feedback and moisture intrusions into the Arctic contributes to slight Arctic
714 surface warming by enhancing downwelling LW radiation to the surface (Taylor et al. 2013; Sejas
715 et al. 2014; Song et al. 2014; Yoshimori et al. 2014; La  n   et al. 2016). However, the combined
716 direct effects of enhanced atmospheric energy convergence into the Arctic and positive water
717 vapor feedback produce weak Arctic warming without large sea-ice loss and enhanced oceanic
718 heat release from October-March. We also found that under global SST warming with fixed Arctic
719 SIC, the Arctic experiences vertically uniform or top-heavy warming, producing a neutral or
720 negative lapse rate feedback. Thus, the lapse rate feedback does not make a large contribution to
721 Arctic warming or AA without the bottom-heavy warming effects of enhanced oceanic energy

722 release associated with sea-ice loss. Lastly, Arctic cloud and surface albedo feedbacks responded
723 weakly to warmer global SST with fixed Arctic SIC in the historical and future cases.

724 In contrast, retreating sea ice produces strong bottom-heavy warming and moistening in
725 autumn and winter due to enhanced oceanic energy release in regions with newly exposed water
726 surfaces, as shown in previous studies (Deser et al. 2010; Screen and Simmonds 2010a, b; Boeke
727 and Taylor 2018; Dai et al. 2019; Dai and Jenkins 2023). Strong lower tropospheric warming
728 enhances Arctic positive lapse rate feedback, which greatly contributes to AA during the cold
729 season (e.g., Jenkins and Dai 2021; Dai and Jenkins 2023). Additionally, bottom-heavy moistening
730 in response to Arctic sea-ice loss has little impact on the TOA radiative flux due to its low
731 sensitivity to lower tropospheric water vapor (Shell et al. 2008; Soden et al. 2008; Pendergrass et
732 al. 2018). Instead, enhanced moistening in the mid-upper troposphere, as in the SST warming runs,
733 increases the Arctic TOA radiative forcing by increasing water vapor's LW absorption in the upper
734 troposphere. Arctic surface albedo feedback activates during the sunlit season in response to sea-
735 ice loss but does not significantly raise surface temperatures in summer. We also find reduced
736 poleward atmospheric energy transport in the northern hemisphere mid-high latitudes due to
737 historical and future Arctic sea-ice loss with fixed global SST, consistent with Hahn et al. (2023).

738 We recognize that there are limitations associated with atmosphere-only model runs as the
739 ocean is treated as a boundary condition. Ocean-atmosphere coupling and the oceanic component
740 of the poleward energy transport have been shown to play important roles in the atmospheric
741 response to sea-ice loss (Deser et al. 2015; Tomas et al. 2016). Thus, future work may compare
742 our feedback calculations to the results from models with a full-depth dynamical ocean to account
743 for ocean feedbacks. Additionally, we emphasize that global SST and Arctic SIC conditions are
744 specified in PAMIP simulations and that many processes influence global SST and Arctic SIC
745 fields in fully-coupled simulations. For example, increased downwelling LW radiation from
746 moisture intrusions into the Arctic or enhanced Arctic atmospheric energy convergence can shape
747 the patterns of future SIC specified in PAMIP simulations (Woods and Caballero 2016; Zhang et
748 al. 2023). Moreover, oceanic heat uptake/release in the simulations with changed SST and fixed
749 SIC may implicitly include changes in oceanic energy convergence as the historical and future
750 SST values were estimated from models with a coupled atmosphere and ocean. Nevertheless, our

751 results help to untangle the influence of background global warming related to global SST changes
752 or large Arctic warming related to sea-ice loss on Arctic climate feedbacks.

753

754 **Acknowledgements**

755 We thank the contributors to the PAMIP project for designing and running the simulations
756 analyzed in this study.

757 **Author Contributions**

758 M. T. Jenkins performed the analysis for this study, made the figures, and wrote the first draft of
759 the manuscript. A. Dai and C. Deser helped improve the study, the manuscript and the figures.

760 **Funding**

761 This work is supported by the National Science Foundation (grants AGS-2015780 and OISE-
762 1743738). The National Center for Atmospheric Research is supported by the National Science
763 Foundation.

764 **Data Availability Statement**

765 The PAMIP model output used in this study can be downloaded from [https://esgf-](https://esgf-node.llnl.gov/search/cmip6/)
766 [node.llnl.gov/search/cmip6/](https://esgf-node.llnl.gov/search/cmip6/).

767 **Ethics Approval**

768 Not applicable.

769 **Consent for Publication**

770 The authors agree to publish the paper in *Climate Dynamics*.

771 **Competing Interests**

772 The authors declare no competing interests.

773

774

775 **References**

- 776 Alexeev VA, Langen PL, Bates JR (2005) Polar amplification of surface warming on an
777 aquaplanet in “ghost forcing” experiments without sea ice feedbacks. *Clim Dyn*, 24:655-
778 666. <https://doi.org/10.1007/s00382-005-0018-3>.
- 779 Audette A, Fajber RA, Kushner PJ, Wu Y, Peings Y, Magnúsdóttir G, et al. (2021) Opposite
780 responses of the dry and moist eddy heat transport into the Arctic in the PAMIP
781 experiments. *Geophys Res Lett*, 48:e2020GL089990.
782 <https://doi.org/10.1029/2020GL089990>.
- 783 Barton NP, Veron DE (2012) Response of clouds and surface energy fluxes to changes in sea-ice
784 cover over the Laptev Sea (Arctic Ocean). *Clim Res*, 54:69-84.
785 <https://doi.org/10.3354/cr01101>.
- 786 Bintanja R, Graversen RG, Hazeleger W (2011) Arctic winter warming amplified by the thermal
787 inversion and consequent low infrared cooling to space. *Nat Geosci*, 4:758–761.
788 <https://doi.org/10.1038/ngeo1285>.
- 789 Block K, Mauritsen T (2013) Forcing and feedback in the MPI-ESM-LR coupled model under
790 abruptly quadrupled CO₂. *J Adv Model Earth Syst*, 5:1-16.
791 <https://doi.org/10.1002/jame.20041>.
- 792 Boeke RC, Taylor PC (2018) Seasonal energy exchange in sea ice retreat regions contributes to
793 differences in projected Arctic warming. *Nat Comm*, 9:5017.
794 <https://doi.org/10.1038/s41467-018-07061-9>.
- 795 Boeke RC, Taylor PC, Sejas SA (2021) On the nature of the Arctic’s positive lapse-rate
796 feedback. *Geophys Res Lett*, 48:e2020GL091109.
797 <https://doi.org/10.1029/2020GL091109>.
- 798 Burt MA, Randall DA, Branson MD (2016) Dark warming. *J Climate*, 29:705-719.
799 <https://doi.org/10.1175/JCLI-D-15-0147.1>.
- 800 Cardinale CJ, Rose BEJ (2023) The increasing efficiency of the poleward energy transport into
801 the Arctic in a warming climate. *Geophys Res Lett*, 50:e2022GL100834.
802 <https://doi.org/10.1029/2022GL100834>.

803 Cai M (2005) Dynamical amplification of polar warming. *Geophys Res Lett*, 32:L22710.
804 <https://doi.org/10.1029/2005GL024481>.

805 Chung P-C, Feldl N (2023) Sea ice loss, water vapor increases, and their interactions with
806 atmospheric energy transport in driving seasonal polar amplification. *J Climate*, online.
807 <https://doi.org/10.1175/JCLI-D-23-0219.1>.

808 Colman R, Soden BJ (2021) Water vapor and lapse rate feedbacks in the climate system. *Rev*
809 *Mod Phys*, 93:045002. <https://doi.org/10.1103/RevModPhys.93.045002>.

810 Curry JA, Schramm JL, Serreze MC, Ebert EE (1995) Water vapor feedback over the Arctic
811 Ocean. *J Geophys Res*, 100:14223-14229. <https://doi.org/10.1029/95JD00824>.

812 Dai A, Luo D, Song M, Liu J (2019) Arctic amplification is caused by sea-ice loss under
813 increasing CO₂. *Nat Comm*, 10:121. <https://doi.org/10.1038/s41467-018-07954-9>.

814 Dai A, Jenkins MT (2023) Relationships among Arctic warming, sea-ice loss, stability, lapse rate
815 feedback, and Arctic amplification. *Clim Dyn*, 61:5217-5232.
816 <https://doi.org/10.1007/s00382-023-06848-x>.

817 Dai H (2021) Roles of surface albedo, surface temperature, and carbon dioxide in the seasonal
818 variation of Arctic amplification. *Geophys Res Lett*, 48:e2020GL090301.
819 <https://doi.org/10.1029/2020GL090301>.

820 Davy R, Griewank P (2023) Arctic amplification has already peaked. *Environ Res Lett*,
821 18:084003. <https://doi.org/10.1088/1748-9326/ace273>.

822 Deser C, Tomas R., Alexander M, Lawrence D (2010) The seasonal atmospheric response to
823 projected Arctic sea ice loss in the late twenty-first century. *J Climate*, 23:333-351.
824 <https://doi.org/10.1175/2009JCLI3053.1>.

825 Deser C, Tomas RA, Sun L (2015) The role of ocean-atmosphere coupling in the zonal-mean
826 atmospheric response to Arctic sea ice loss. *J Climate*, 28:2168-2186.
827 <https://doi.org/10.1175/JCLI-D-14-00325.1>.

828 Dwyer JG, Biasutti M, Sobel AH (2012) Projected changes in the seasonal cycle of surface
829 temperature. *J Climate* 25:6359-6374. <https://doi.org/10.1175/JCLI-D-11-00741.1>.

830 Eastman R, Warren SG (2010) Interannual variations of Arctic cloud types in relation to sea ice.
831 J. Climate 23:4216-4232. <https://doi.org/10.1175/2010JCLI3492.1>.

832 England MR, Eisenman I, Lutsko NJ, Wagner TJ (2021) The recent emergence of Arctic
833 amplification. Geophys Res Lett, 48:e2021GL094086.
834 <https://doi.org/10.1029/2021GL094086>.

835 Fasullo JT, Trenberth KE (2008) The annual cycle of the energy budget. Part I: Global mean and
836 land-ocean exchanges. J Climate, 21:2297-2312.
837 <https://doi.org/10.1175/2007JCLI1935.1>.

838 Feldl N, Anderson BT, Bordoni S (2017a) Atmospheric eddies mediate lapse rate feedback and
839 Arctic amplification. J Climate, 30:9213-9224. <https://doi.org/10.1175/JCLI-D-16-0706.1>.

840

841 Feldl N, Bordoni S, Merlis TM (2017b) Coupled high-latitude climate feedbacks and their
842 impact on atmospheric heat transport. J Climate, 30:189-201.
843 <https://doi.org/10.1175/JCLI-D-16-0324.1>.

844 Feldl N, Po-Chedley S, Singh HKA, Hay S, Kushner PJ (2020) Sea ice and atmospheric
845 circulation shape the high-latitude lapse rate feedback. npj Climate and Atmospheric
846 Science, 3:41. <https://doi.org/10.1038/s41612-020-00146-7>.

847 Ghatak D, Miller J (2013) Implications for Arctic amplification of changes in the strength of the
848 water vapor feedback. J Geophys Res Atmos, 118:7569-7578.
849 <https://doi.org/10.1002/jgrd.50578>.

850 Gong T, Feldstein S, Lee S (2017) The role of downward infrared radiation in the recent Arctic
851 winter warming trend. J Climate, 30:4937-4949. <https://doi.org/10.1175/JCLI-D-16-0180.1>.

852

853 Goosse H, Kay JE, Armour KC, Bodas-Salcedo A, Chepfer H, Docquier D, et al. (2018)
854 Quantifying climate feedbacks in polar regions. Nat Comm, 9:1919.
855 <https://doi.org/10.1038/s41467-018-04173-0>.

856 Hay S, Kushner PJ, Blackport R, McCusker KE, Oudar T, Sun L, et al. (2022) Separating the
857 influences of low-latitude warming and sea-ice loss on northern hemisphere climate
858 change. *J Climate*, 35:2327-2349. <https://doi.org/10.1175/JCLI-D-21-0180.1>.

859 Hahn LC, Armour KC, Zelinka MD, Bitz CM, Donohoe A (2021) Contributions to polar
860 amplification in CMIP5 and CMIP6 models. *Front Earth Sci*, 9:710036.
861 <https://doi.org/10.3389/feart.2021.710036>.

862 Hahn LC, Armour KC, Battisti DS, Eisenman I, Bitz CM (2022) Seasonality in Arctic warming
863 driven by sea ice effective heat capacity. *J. Climate*, 35:1629-1642.
864 <https://doi.org/10.1175/JCLI-D-21-0626.1>.

865 Hahn LC, Armour KC, Battisti DS, Donohoe A, Fajber R (2023) Seasonal changes in
866 atmospheric heat transport to the Arctic under increased CO₂. *Geophys Res Lett*,
867 50:e2023GL105156. <https://doi.org/10.1029/2023GL105156>.

868 Hall A (2004) The role of surface albedo feedback in climate. *J Climate*, 17:1550-1568.
869 [https://doi.org/10.1175/1520-0442\(2004\)017%3C1550:TROSAF%3E2.0.CO;2](https://doi.org/10.1175/1520-0442(2004)017%3C1550:TROSAF%3E2.0.CO;2).

870 Henry M, Merlis TM, Lutsko NJ, Rose BEJ (2021) Decomposing the drivers of polar
871 amplification with a single-column model. *J Climate*, 34:2355-2365.
872 <https://doi.org/10.1175/JCLI-D-20-0178.1>.

873 Hu X, Liu Y, Kong Y, and Yang Q (2022) A quantitative analysis of the source of inter-model
874 spread in Arctic surface warming response to increased CO₂ concentration. *Geophys Res*
875 *Lett*, 49:e2022GL100034. <https://doi.org/10.1029/2022GL100034>.

876 Hwang Y-T, Frierson DMW (2010) Increasing atmospheric poleward energy transport with
877 global warming. *Geophys Res Lett*, 37:L24807. <https://doi.org/10.1029/2010GL045440>.

878 Hwang Y-T, Frierson DMW, Kay JE (2011) Coupling between Arctic feedbacks and changes in
879 poleward energy transport. *Geophys Res Lett*, 38:L17704.
880 <https://doi.org/10.1029/2011GL048546>.

881 Janoski TP, Previdi M, Chiodo G, Smith KL, Polvani LM (2023) Ultrafast Arctic amplification
882 and its governing mechanisms. *Environ. Res.: Climate*, 2:035009.
883 <https://doi.org/10.1088/2752-5295/ace211>.

884 Jenkins M, Dai A (2021) The impact of sea-ice loss on Arctic climate feedbacks and their role
885 for Arctic amplification. *Geophys Res Lett*, 48:e2021GL094599.
886 <https://doi.org/10.1029/2021GL094599>.

887 Jenkins MT, Dai A (2022) Arctic climate feedbacks in ERA5 reanalysis: Seasonal and spatial
888 variations and the impact of sea-ice loss. *Geophys Res Lett*, 49:e2022GL099263.
889 <https://doi.org/10.1029/2022GL099263>.

890 Jenkins MT, Dai A, Deser C (2023) Seasonal variations and spatial patterns of Arctic cloud
891 changes in association with sea-ice loss during 1950-2019 in ERA5. *J Climate*,
892 <https://doi.org/10.1175/JCLI-D-23-0117.1>.

893 Kay JE, Gettelman A (2009) Cloud influence on and response to seasonal Arctic sea-ice loss. *J*
894 *Geophys Res*, 114:D18204. <https://doi.org/10.1029/2009JD011773>.

895 Kay JE, L'Ecuyer T, Chepfer H, Loeb N, Morrison A, Cesana G (2016) Recent advances in
896 Arctic cloud and climate research. *Curr Clim Change Rep*, 2:159-169.
897 <https://doi.org/10.1007/s40641-016-0051-9>.

898 Kumar A, Perlwitz J, Eischeid J, Quan X, Xu T, Zhang T, et al. (2010) Contribution of sea ice
899 loss to Arctic amplification. *Geophys Res Lett*, 37:L21701.
900 <https://doi.org/10.1029/2010GL045022>.

901 Laîné A, Yoshimori M, Abe-Ouchi A (2016) Surface Arctic amplification factor in CMIP5
902 models: Land and oceanic surfaces and seasonality. *J Climate*, 29:3297-3316.
903 <https://doi.org/10.1175/JCLI-D-15-0497.1>.

904 Liang Y-C, Polvani LM, Mitevski I (2022) Arctic amplification, and its seasonal migration, over
905 a wide range of abrupt CO₂ forcing. *npj Climate and Atmospheric Science*, 5:14.
906 <https://doi.org/10.1038/s41612-022-00228-8>.

907 Linke O, Quaas J, Baumer F, Becker S, Chylik J, Dahlke S, et al. (2023a) Constraints on
908 simulated past Arctic amplification and lapse rate feedback from observations. *Atmos.*
909 *Chem. Phys.* 23:9963–9992. <https://doi.org/10.5194/acp-23-9963-2023>.

910 Linke O, Feldl N, Quaas J (2023b) Current-climate sea ice amount and seasonality as constraints
911 for future Arctic amplification. *Environ Res: Climate*, 2:045003.
912 <https://doi.org/10.1088/2752-5295/acf4b7>.

913 Liu Y, Key JR, Liu Z, Wang X, Vavrus SJ (2012) A cloudier Arctic expected with diminishing
914 sea ice. *Geophys Res Lett*, 39:L05705. <https://doi.org/10.1029/2012GL051251>.

915 Merlis TM, Henry M (2018) Simple estimates of polar amplification in moist diffusive energy
916 balance models. *J Climate*, 31:5811-5824. <https://doi.org/10.1175/JCLI-D-17-0578.1>.

917 Middlemas EA, Kay JE, Medeiros BM, Maroon EA (2020) Quantifying the influence of cloud
918 radiative feedbacks on Arctic surface warming using cloud locking in an Earth system
919 model. *Geophys Res Lett*, 47:e2020GL089207. <https://doi.org/10.1029/2020GL089207>.

920 Monroe EE, Taylor PC, Boisvert LN (2021) Arctic cloud response to a perturbation in sea ice
921 concentration: The north water polynya. *J Geophys Res Atmos*, 126:e2020JD034409.
922 <https://doi.org/10.1029/2020JD034409>.

923 Morrison AL, Kay JE, Chepfer H, Guzman R, Yettella V (2018) Isolating the liquid cloud
924 response to recent Arctic sea ice variability using spaceborne lidar observations. *J*
925 *Geophys Res Atmos*, 123:473-490. <https://doi.org/10.1002/2017JD027248>.

926 Morrison AL, Kay JE, Frey WR, Chepfer H, Guzman R (2019) Cloud response to Arctic sea ice
927 loss and implication for future feedback in the CESM1 climate model. *J Geophys Res*
928 *Atmos*, 124:1003-1020. <https://doi.org/10.1029/2018JD029142>.

929 Oort AH, Vonder Haar TH (1976) On the observed annual cycle in the ocean-atmosphere heat
930 balance over the northern hemisphere. *J Phys Oceanogr*, 6:781-800.
931 [https://doi.org/10.1175/1520-0485\(1976\)006%3C0781:OTOACI%3E2.0.CO;2](https://doi.org/10.1175/1520-0485(1976)006%3C0781:OTOACI%3E2.0.CO;2).

932 Palm SP, Strey ST, Spinhirne J, and Markus T (2010) Influence of Arctic sea-ice extent and
933 polar cloud fraction and vertical structure and implications for regional climate. *J*
934 *Geophys Res*, 115:D21209. <https://doi.org/10.1029/2010JD013900>.

935 Pendergrass AG, Conley A, Vitt FM (2018) Surface and top-of-atmosphere radiative feedback
936 kernels for CESM-CAM5. *Earth Sys Sci Data*, 10:317-324. [https://doi.org/10.5194/essd-](https://doi.org/10.5194/essd-10-317-2018)
937 [10-317-2018](https://doi.org/10.5194/essd-10-317-2018).

938 Perlwitz J, Hoerling M, Dole R (2015) Arctic tropospheric warming: causes and linkages to
939 lower latitudes. *J Climate*, 28:2154-2167. <https://doi.org/10.1175/JCLI-D-14-00095.1>.

940 Pithan F, Mauritsen T (2014) Arctic amplification dominated by temperature feedbacks in
941 contemporary climate models. *Nat Geosci*, 7:181-184.
942 <https://doi.org/10.1038/NGEO2071>.

943 Previdi M, Janoski TP, Chiodo G, Smith KL, Polvani LM (2020) Arctic amplification: A rapid
944 response to radiative forcing. *Geophys Res Lett*, 47:e2020GL089933.
945 <https://doi.org/10.1029/2020GL089933>.

946 Roe GH, Feldl N, Armour KC, Hwang Y-T, Frierson DMW (2015) The remote impacts of
947 climate feedbacks on regional climate predictability. *Nat Geosci*, 8:135-139.
948 <https://doi.org/10.1038/NGEO2346>.

949 Screen JA, Simmonds I (2010a) The central role of diminishing sea ice in recent Arctic
950 temperature amplification. *Nature*, 464:1334-1337. <https://doi.org/10.1038/nature09051>.

951 Screen JA, Simmonds I (2010b) Increasing fall-winter energy loss from the Arctic Ocean and its
952 role in Arctic temperature amplification. *Geophys Res Lett*, 37:L16707.
953 <https://doi.org/10.1029/2010GL044136>.

954 Screen JA, Deser C, Simmonds I, Tomas R (2014) Atmospheric impacts of Arctic sea-ice loss,
955 1979-2009: Separating forced change from atmospheric internal variability. *Clim Dyn*,
956 43:333-344. <https://doi.org/10.1007/s00382-013-1830-9>.

957 Schweiger AJ, Lindsay RW, Vavrus S, Francis JA (2008) Relationships between Arctic sea ice
958 and clouds during autumn. *J Climate*, 21:4799-4810.
959 <https://doi.org/10.1175/2008JCLI2156.1>.

960 Sejas SA, Cai M, Hu A, Meehl GA, Washington W, Taylor PC (2014) Individual feedback
961 contributions to the seasonality of surface warming. *J Climate*, 27:5653-5669.
962 <https://doi.org/10.1175/JCLI-D-13-00658.1>.

963 Sejas SA, Taylor PC, Cai M (2018) Unmasking the negative greenhouse effect over the Antarctic
964 Plateau. *npj Climate and Atmospheric Science*, 1:17. <https://doi.org/10.1038/s41612-018-0031-y>.
965

966 Sejas SA, Taylor PC (2023) The role of sea ice in establishing the seasonal Arctic warming
967 pattern. *Environ Res: Climate*, 2:035008. <https://doi.org/10.1088/2752-5295/ace20f>.

968 Serreze MC, Barry RG (2011) Processes and impacts of Arctic amplification: A research
969 synthesis. *Global and Planetary Change*, 77:85-96.
970 <https://doi.org/10.1016/j.gloplacha.2011.03.004>.

971 Shell KM, Kiehl JT, Shields CA (2008) Using the radiative kernel technique to calculate climate
972 feedbacks in NCAR's community atmospheric model. *J Climate*, 21:2269–2282.
973 <https://doi.org/10.1175/2007JCLI2044.1>.

974 Smith DM, Screen JA, Deser C, Cohen J, Fyfe JC, García-Serrano J, et al. (2019) The polar
975 amplification model intercomparison project (PAMIP) contribution to CMIP6:
976 Investigating the causes and consequences of polar amplification. *Geosci Model Dev*,
977 12:1139-1164. <https://doi.org/10.5194/gmd-12-1139-2019>.

978 Soden BJ, Held IM, Colman R, Shell KM, Kiehl JT, Shields CA (2008) Quantifying climate
979 feedbacks using radiative kernels. *J. Climate*, 21:3504-3520.
980 <https://doi.org/10.1175/2007JCLI2110.1>.

981 Soldatenko S (2021) Effects of global warming on the poleward heat transport by non-stationary
982 large-scale atmospheric eddies, and feedbacks affecting the formation of the Arctic
983 climate. *J Mar Sci Eng*, 9:867. <https://doi.org/10.3390/jmse9080867>.

984 Song X, Zhang GJ, Cai M (2014) Quantifying contributions of climate feedbacks to tropospheric
985 warming in the NCAR CCSM3.0. *Clim Dyn*, 42:901-917.
986 <https://doi.org/10.1007/s00382-013-1805-x>.

987 Stuecker MF, Bitz CM, Armour KC, Proistosescu C, Kang SM, Xie S-P, et al. (2018) Polar
988 amplification dominated by local forcing and feedbacks. *Nat Clim Change*, 8:1076-1081.
989 <https://doi.org/10.1038/s41558-018-0339-y>.

990 Sun L, Perlwitz J, Hoerling M (2016) What caused the recent “Warm Arctic, Cold Continents”
991 trend pattern in winter temperatures? *Geophys Res Lett*, 43:5345-5352.
992 <https://doi.org/10.1002/2016GL069024>.

- 993 Taylor PC, Cai M, Hu A, Meehl J, Washington W, Zhang GJ (2013) A decomposition of
994 feedback contributions to polar warming amplification. *J Climate*, 26:7023-7043.
995 <https://doi.org/10.1175/JCLI-D-12-00696.1>.
- 996 Taylor PC, Kato S, Xu K-M, Cai M (2015) Covariance between Arctic sea ice and clouds within
997 atmospheric state regimes at the satellite footprint level. *J Geophys Res Atmos*,
998 120:12656-12678. <https://doi.org/10.1002/2015JD023520>.
- 999 Taylor PC, Hegyi BM, Boeke RC, Boisvert LN (2018) On the increasing importance of air-sea
1000 exchanges in a thawing Arctic: A review. *Atmosphere*, 9:41.
1001 <https://doi.org/10.3390/atmos9020041>.
- 1002 Taylor PC, Boeke RC, Boisvert LN, Feldl N, Henry M, Huang Y, et al. (2022) Process drivers,
1003 inter-model spread, and the path forward: A review of amplified Arctic warming. *Front.*
1004 *Earth Sci.*, 9:758361. <https://doi.org/10.3389/feart.2021.758361>.
- 1005 Taylor PC, Monroe E (2023) Isolating the surface type influence on Arctic low-clouds. *J*
1006 *Geophys Res Atmos*, 128:e2022JD038098. <https://doi.org/10.1029/2022JD038098>.
- 1007 Tomas RA, Deser C, Sun L (2016) The role of ocean heat transport in the global climate
1008 response to projected Arctic sea ice loss. *J Climate*, 29:6841-6859.
1009 <https://doi.org/10.1175/JCLI-D-15-0651.1>.
- 1010 Trenberth KE, Solomon A (1994) The global heat balance: heat transports in the atmosphere and
1011 ocean. *Clim Dyn*, 10:107-134. <https://doi.org/10.1007/BF00210625>.
- 1012 Trenberth KE (1997) Using atmospheric budgets as a constraint on surface fluxes. *J Climate*,
1013 10:2796-2809. [https://doi.org/10.1175/1520-
1014 0442\(1997\)010%3C2796:UABAAC%3E2.0.CO;2](https://doi.org/10.1175/1520-0442(1997)010%3C2796:UABAAC%3E2.0.CO;2).
- 1015 Vavrus S (2004) The impact of cloud feedbacks on Arctic climate under greenhouse forcing. *J*
1016 *Climate*, 17:603-615. [https://doi.org/10.1175/1520-
1017 0442\(2004\)017%3C0603:TIOCF0%3E2.0.CO;2](https://doi.org/10.1175/1520-0442(2004)017%3C0603:TIOCF0%3E2.0.CO;2).
- 1018 Virgin JG, Smith KL (2019) Is Arctic amplification dominated by regional radiative forcing and
1019 feedbacks: Perspectives from the world-avoided scenario. *Geophys Res Lett*, 46:7708-
1020 7717. <https://doi.org/10.1029/2019GL082320>.

- 1021 Walsh JE (2014) Intensified warming of the Arctic: Causes and impacts on middle latitudes.
1022 Global and Planetary Change, 117:52-63.
1023 <https://doi.org/10.1016/j.gloplacha.2014.03.003>.
- 1024 Wetherald RT, Manabe S (1988) Cloud feedback processes in a general circulation model. J
1025 Atmos Sci, 45:1397-1415. [https://doi.org/10.1175/1520-
1026 0469\(1988\)045%3C1397:CFPIAG%3E2.0.CO;2](https://doi.org/10.1175/1520-0469(1988)045%3C1397:CFPIAG%3E2.0.CO;2).
- 1027 Winton M (2006) Amplified Arctic climate change: What does surface albedo feedback have to
1028 do with it? Geophys Res Lett, 29:4473-4485. <https://doi.org/10.1029/2005GL025244>.
- 1029 Woods C, Caballero R (2016) The role of moist intrusions in winter Arctic warming and sea ice
1030 decline. J Climate, 29:4473-4485. <https://doi.org/10.1175/JCLI-D-15-0773.1>.
- 1031 Yoshimori M, Wantanabe M, Abe-Ouchi A, Shiogama H, Ogura T (2014) Relative contribution
1032 of feedback processes to Arctic amplification of temperature change in MIROC GCM.
1033 Clim Dyn, 42:1613-1630. <https://doi.org/10.1007/s00382-013-1875-9>.
- 1034 Zhang P, Chen G, Ting M, Leung LR, Guan B, Li L (2023) More frequent atmospheric river
1035 slow the seasonal recovery of Arctic sea ice. Nat Clim Change, 13:266-273.
1036 <https://doi.org/10.1038/s41558-023-01599-3>.
- 1037 Zhou S-N, Liang Y-C, Mitevski I, Polvani LM (2023) Stronger Arctic amplification produced by
1038 decreasing, not increasing, CO₂ concentrations. Environ Res: Climate, 2:045001.
1039 <https://doi.org/10.1088/2752-5295/aceea2>.